

Upper Bound on Thermal Gravitational Wave Backgrounds from Hidden Sectors

Marco Drewes^{*a}, Yannis Georis^{†a}, Juraj Klarić^{‡b,c,d,a}, and Philipp Klose^{§e,f}

^aCentre for Cosmology, Particle Physics, and Phenomenology,

Université catholique de Louvain, Louvain-la-Neuve B-1348, Belgium

^bInstitute for Theoretical Physics Amsterdam and Delta Institute for Theoretical Physics,
University of Amsterdam, Science Park 904, 1098 XH Amsterdam, The Netherlands

^cNikhef, Theory Group, Science Park 105, 1098 XG, Amsterdam, The Netherlands

^dUniversity of Zagreb, Faculty of Science, Department of Physics, 10000 Zagreb, Croatia

^eInstitute for Theoretical Physics, Albert Einstein Center for Fundamental Physics, University of Bern

^fFakultät für Physik, Universität Bielefeld

Abstract

Hot viscous plasmas unavoidably emit a gravitational wave background, similar to electromagnetic black body radiation. We study the contribution from hidden particles to the diffuse background emitted by the primordial plasma in the early universe. While this contribution can easily dominate over that from Standard Model particles, we find that both are capped by a generic upper bound that makes them difficult to detect with interferometers in the foreseeable future. We illustrate our results for axion-like particles and heavy neutral leptons. Finally, our results suggest that previous works overestimated the gravitational wave background from particle decays out of thermal equilibrium.

^{*}marco.drewes@uclouvain.be

[†]yannis.georis@uclouvain.be

[‡]juraj.klarić@nikhef.nl

[§]pklose@physik.uni-bielefeld.de

Contents

1	Introduction	3
2	Gravitational waves from thermal fluctuations	4
2.1	Enhancement due to feeble interactions	5
2.2	Present day spectrum	6
3	Gravitational wave production rates	8
3.1	Feebly interacting particles	8
3.2	Approximate formulae for phenomenology	9
4	Phenomenology	11
4.1	Generic features	11
4.2	Model-independent upper bound	13
4.3	Analytic estimates of the high-temperature background	15
4.3.1	Renormalizable interactions	15
4.3.2	Non-renormalizable interactions	16
5	Explicit examples	20
5.1	Axion-like particles	20
5.2	Heavy neutral leptons	23
6	Discussion and conclusion	24
	Appendices	28
A	GW production rate from fermions	28
B	Finite temperature spectral function	31
C	Supplementary formulae for backgrounds from non-renormalizable interactions	32
D	More general cosmic histories	35

1 Introduction

Primordial gravitational wave backgrounds (GWBs) are a tantalizing probe of new physics in the early universe that can complement searches for hints in cosmology or at particle physics experiments. In particular, the prospective Laser Interferometer Space Antenna (LISA) [1] will likely be sensitive to gravitational wave (GW) signatures of the strong first-order phase transitions predicted in various popular new physics models [2–5]. The observation of such backgrounds is a major physics motivation of LISA and various other proposed GW detectors, such as the Einstein Telescope [6, 7], Deci-hertz Interferometer Gravitational wave Observatory (DECIGO) [8, 9] and u-DECIGO [10, 11], and Big Bang Observer [12–14]. Recently, significant attention has also turned towards the possibility of detecting ultra high-frequency GWs, see e.g. [15] and references therein for particular examples of proposed searches. One advantage of this kind of search is that the known sources of the astrophysical GWB are not small enough to produce GWs at high frequencies above $\sim 10^4$ Hz [15].

While strong first order phase transitions and other violent out-of-equilibrium phenomena that may have occurred in the early universe are amongst the most promising sources of primordial GWBs [16–21], a deviation from thermal equilibrium is not a strict requirement for GW production: Any viscous plasma produces GWs due to microscopic thermal fluctuations [22–24]. The resulting background is generically expected to be much weaker than that of out-of-equilibrium processes, but it is much harder to avoid since the mechanism does not rely on any deviation from the standard cosmology. Thermal fluctuations are expected to be a primary source of the Standard Model (SM) contribution to the primordial GWB [22, 23], and it has been pointed out that this contribution effectively measures the largest temperature of the early universe plasma after inflation [23, 25].

In general, thermal fluctuations produce a black-body-like GW spectrum that peaks at momenta $k \sim \pi T$ and exhibits a long tail extending to much smaller frequencies. Close to the peak, the fluctuations are best described as the result of particle collisions, but this description breaks down for sufficiently small frequencies, where hydrodynamics becomes applicable instead. In this domain, the production rate exhibits a universal $\propto k^3$ frequency scaling. Hydrodynamics is appropriate e.g. for computing the SM contribution to primordial GWBs with frequencies in the LISA window $10^{-4} \text{ Hz} < f < 10^{-1} \text{ Hz}$ [5, 23, 25], and the same can be true for contributions from many extensions of the SM. Since the size of the relevant hydrodynamic fluctuations generically scales as the mean free path of the most weakly interacting plasma constituent [22, 23, 26–28], GW production can be enhanced if these extensions contain particles whose interactions are weaker than the SM U(1) hypercharge gauge interactions. The existence of such feebly interacting particles [29] is predicted by various theoretical ideas to address the shortcomings of the SM, either as a standalone or as a component of an extended hidden sector that couples to the SM only via portal interactions, cf. e.g. [29–32] and references therein. These particles can be produced thermally or via non-thermal processes such as (p)reheating or the decay of heavier new particles. A similar enhancement of GWBs due to the presence of feebly interacting particles has been pointed out in the context of strong first-order phase-transitions [33], and the production of gravitational waves from hydrodynamic fluctuations has also been considered in the context of axion-like warm inflation [34, 35].

In the present work, we focus on GWBs produced in thermal equilibrium during the radiation dominated period of the early universe. The primary quantity determining the production rate

in the hydrodynamic regime is the shear viscosity η . The shear viscosities of various generic $U(N)$ and $SU(N)$ gauge theories are well established in the literature [36–38], and there also exist prior results for the viscosity of a single, feebly interacting (pseudo-)scalar [34, 39]. We adapt the strategy in [34, 39] to compute the shear viscosity of a massive feebly interacting fermion ψ , and combine this result with these prior computations to study the GWB due to generic feebly interacting particles, pointing out the existence of a model-independent upper bound. As specific examples, we then consider axion-like particles (ALPs) and heavy neutral leptons (HNLs).

This article is structured as follows: In section 2, we briefly review the mechanism for thermal GW production. We present the rates for GW production from hidden scalars and fermions in section 3, where the latter is based on the computation in appendix A. In section 4, we then discuss the phenomenological implications for GWBs from feebly interacting particles, including a model-independent upper bound (section 4.2) and useful approximate formulae to compute the GWB in the high temperature regime (section 4.3). We illustrate these for two popular hidden particles in section 5, namely ALPs and HNLs. Section 6 concludes the paper.

2 Gravitational waves from thermal fluctuations

GWs are traceless-transverse tensor perturbations to the metric. The relevant line-element for a spatially flat FLRW background cosmology is

$$ds^2 = dt^2 - a^2(\delta_{ij} + h_{ij})dx^i dx^j, \quad h_i^i = \partial_i h_{ij} = 0, \quad (1)$$

where $a = a(t)$ is the scale-factor of the universe and h_{ij} the graviton field. It evolves according to the linearized wave-equation

$$\ddot{h}_{ij} + 3H\dot{h}_{ij} - \frac{\nabla^2 h_{ij}}{a^2} = \frac{16\pi T_{ij}}{a^2 m_{\text{Pl}}^2}, \quad (2)$$

where $m_{\text{Pl}} \equiv 1/\sqrt{G} \approx 1.22 \cdot 10^{19}$ GeV is the Planck mass, and T_{ij} the traceless-transverse contribution to the Einstein stress-energy tensor.

In the following, we focus on the production of gravitational waves at sub-horizon scales due to microphysical fluctuations in a thermalized early universe plasma. In this case, the Hubble rate $H \equiv \dot{a}/a$ is small compared to the redshifted GW frequency $2\pi f a_0/a = k$, where f is the frequency at present time, k the physical graviton momentum, and a_0 the scale factor at present time. It can be shown that the spectral energy density e_{gw} evolves according to the equation of motion [22, 23, 25]

$$\frac{d\dot{e}_{\text{gw}}}{d \ln f} + 4H \frac{de_{\text{gw}}}{d \ln f} = 16\pi^2 \left(\frac{f a_0}{a}\right)^3 \frac{\Pi(2\pi f a_0/a)}{m_{\text{Pl}}^2}, \quad e_{\text{gw}} \equiv \frac{m_{\text{Pl}}^2}{32\pi} \langle \dot{h}^{ij}(t, \mathbf{0}) \dot{h}_{ij}(t, \mathbf{0}) \rangle_\rho, \quad (3)$$

where the production rate

$$\Pi(k) = \frac{1}{2} \int dt d^3 \mathbf{x} e^{i(k t - \mathbf{k} \cdot \mathbf{x})} \mathbb{L}^{ij;kl} \langle \{T_{ij}(t, \mathbf{x}), T_{kl}(0, \mathbf{0})\} \rangle_\rho, \quad \mathbf{k} \cdot \mathbf{x} = \delta_{ij} k^i x^j, \quad k^2 = \delta_{ij} k^i k^j \quad (4)$$

is computed in locally Minkowskian coordinates. Accordingly, the spatial Lorentz indices are raised and lowered using the Kronecker delta δ_{ij} , while the projector

$$\mathbb{L}_{ij;kl} = \frac{1}{2}(\mathbb{L}_{ik}\mathbb{L}_{jl} + \mathbb{L}_{il}\mathbb{L}_{jk} - \mathbb{L}_{ij}\mathbb{L}_{kl}) , \quad \mathbb{L}_{ij} = \delta_{ij} - \frac{k_i k_j}{k^2} , \quad (5)$$

ensures that only the traceless-transverse components of T_{ij} contribute. Working in the Heisenberg picture, the quantum-statistical average $\langle \mathcal{O} \rangle_\rho \equiv \text{tr}\{\rho \mathcal{O}\}$, where ρ is the von Neumann density matrix, encodes information about the state of the early universe plasma, including e.g. the temperature, at the time of production.

2.1 Enhancement due to feeble interactions

The stress-energy tensor is a composite operator constructed from the various elementary quantum fields in the theory. At sufficiently large distances, it is possible to capture the dynamics of systems close to local thermal equilibrium in a model-independent way by expanding the tensor around its perfect fluid ansatz. Choosing a frame in which the fluid three-velocity v^i is small, this defines the hydrodynamic stress-energy tensor

$$T_0^0 = e , \quad T_0^i = (e + p)v^i , \quad T_i^j = [p - \zeta(\nabla \mathbf{v})]\delta_i^j - \eta \left[\partial_i v^j + \partial^j v_i - \frac{2}{3}\delta_i^j(\nabla \mathbf{v}) \right] , \quad (6)$$

where e is the local energy density, p the pressure, ζ the bulk viscosity, and η the shear viscosity. The hydrodynamic ansatz (6) is consistent at energy scales $\omega \gg \Gamma$, where $\Gamma \sim k^2 \eta / T^4$ is the damping rate of sound waves with wavenumber $k = \omega / c_s$. Using that the speed of sound $c_s \approx 1/\sqrt{3}$ is approximately independent of k , one finds the equivalent condition $\omega \eta \ll T^4$. In this regime, the shear viscosity η measures the size of the traceless-transverse contributions to the stress-energy tensor. Indeed, the production rate Π turns out to obey the Kubo formula [22]

$$\lim_{k \rightarrow 0} \Pi = 8T\eta . \quad (7)$$

The shear viscosity is generically expected to scale as the mean free path l_{av} of the most weakly interacting plasma constituent [26–28],

$$\eta \sim l_{\text{av}} v_{\text{av}} T^4 \sim T^4 / \Upsilon , \quad (8)$$

where v_{av} is the average velocity associated with the relevant particle species and Υ is its total width, which is connected to the mean free path via the optical theorem. In other words, particles with feeble interactions, and therefore long free paths, tend to dominate GW production in the regime $\omega \eta \ll T^4$, making GWs a potentially promising probe for hidden sectors.

At first glance, the scaling of (8) also seems to imply that the shear viscosity, and with it the GW production rate, diverges in the limit $\Upsilon \rightarrow 0$, where the particle is in fact completely sterile. However, this scaling is only valid in the hydrodynamic limit $k \ll \Upsilon$. For smaller widths $\Upsilon \lesssim k$, one instead recovers the naively expected scaling $\Pi \propto \Upsilon$, with no enhancement for feebly interacting particles. Hence, as expected, feebly interacting particles dominate primordial GW production in the hydrodynamic regime but not necessarily in other regimes.

2.2 Present day spectrum

To solve equation (3), one has to fix the time-dependence of the scale factor a , which is connected to the evolution of the early universe plasma via conservation of the comoving entropy density, $\partial_t[a^3(s + s_h)] = 0$, where s and s_h respectively denote the SM and hidden sector contributions to the entropy density. Neglecting entropy transfer between the two sectors,¹ entropy conservation applies separately to s and s_h , so that

$$\partial_t(a^3 s) = 0, \quad s = \frac{2\pi^2}{45} g_s(T) T^3, \quad \frac{aT}{a_0 T_0} = \left[\frac{g_s(T_0)}{g_s(T)} \right]^{1/3}, \quad (9)$$

where T is the temperature of the SM plasma, $g_s = g_s(T)$ the effective number of radiation degrees of freedom as measured by the SM entropy density, and T_0 the temperature at present time. We assume that the SM dominates the overall energy budget of the universe, so that the temperature evolves according to the standard cosmology,

$$\frac{dT}{dt} = -\frac{g_s}{g_c} \frac{T^3}{m_0}, \quad m_0 \equiv m_{\text{Pl}} \left[\frac{4\pi^3 g_\rho}{45} \right]^{-1/2}, \quad \rho = g_\rho \frac{\pi^2}{30} T^4, \quad c = g_c \frac{2\pi^2}{15} T^3, \quad (10)$$

where m_0 tracks the comoving temperature, and g_ρ and g_c denote the effective number of radiation degrees of freedom as measured by the SM energy density ρ and heat capacity c . This assumption is reasonable if the total number of hidden sector degrees of freedom is small compared to the number of SM degrees of freedom. Combining equations (3), (9), and (10), the present time stochastic GWB from thermal fluctuations is [23, 25]

$$h^2 \Omega_{\text{gw}}(f) \equiv \frac{h^2}{e_{\text{crit}}} \frac{de_{\text{gw}}}{d \ln f} = \frac{2880\sqrt{5}\pi}{\pi^2} h^2 \Omega_\gamma \frac{f^3}{T_0^3} \int_{T_{\text{min}}}^{T_{\text{max}}} \frac{dT'}{m_{\text{Pl}}} \frac{g_c(T') [g_s(T_0)]^{1/3}}{[g_\rho(T')]^{1/2} [g_s(T')]^{4/3}} \frac{\Pi(2\pi f a_0/a')}{8T'^4}, \quad (11)$$

where

$$h^2 \Omega_\gamma = \frac{h^2}{e_{\text{crit}}} \frac{2\rho}{g_\rho(T_0)}, \quad e_{\text{crit}} = \frac{3H_0^2 m_{\text{Pl}}^2}{8\pi}, \quad H_0 = 100 \text{ km s}^{-1} \text{ Mpc}^{-1} \cdot h \quad (12)$$

is the present day photon energy density, normalized to the critical energy density e_{crit} , H_0 the present day Hubble rate, and h the reduced Hubble rate. Assuming that the bulk of the GWB is produced at temperatures well above the electroweak phase transition, one has $g_c(T') = g_s(T') = g_\rho(T') = 106.75$. Also using [43–45]

$$h^2 \Omega_\gamma = 2.4728(21) \cdot 10^{-5}, \quad g_s(T_0) = 3.931(4), \quad T_0 = 2.7255(6) \text{ K} = 3.5682(7) \cdot 10^{11} \text{ Hz}, \quad (13)$$

¹ This assumption is not always valid. In particular, heavy new particle decays, e.g. in conjunction with a period of early matter domination [40–42], can inject entropy into the SM plasma. The net effect of such an entropy injection would be an additional dilution of primordial GW signals, which we neglect.

one obtains²

$$h^2 \Omega_{\text{gw}}(f) \approx 2.02 \cdot 10^{-38} \times \left(\frac{f}{\text{Hz}} \right)^3 \times \int_{T_{\min}}^{T_{\max}} \frac{dT'}{m_{\text{Pl}}} \frac{\Pi(2\pi f a_0/a')}{8T'^4} . \quad (15)$$

This is the main expression we use in the remainder of this work. If the production rate Π and the integration bounds T_{\max} and T_{\min} are independent of f , the prefactor results in the characteristic $\propto f^3$ frequency shape associated with backgrounds from hydrodynamic fluctuations. This has also been observed e.g. within the context of GWs from post-inflationary phases stiffer than radiation [46] and axion-like inflation [35].

Equation (11) explicitly relies on our assumptions that the SM is in kinetic equilibrium and dominates the overall energy budget, while expression (15) further assumes that its number of radiation degrees of freedom also evolves according to standard cosmic history. This implies that expression (15), and subsequently our results in section 4, only applies to GWBs produced after inflation and after the plasma of inflaton decay products has equilibrated cf. e.g. [47].³ While GWBs from earlier epochs can be important, and although, in principle, the present formalism can be used to compute them, we stick to (11) and only briefly comment on GW production during (p)reheating at the end. That being said, equations (11) and (15) do not necessarily require the hidden sector to be in thermal equilibrium. In fact, they contain no assumption about the hidden sector phase space distribution functions except that their total energy density has to be small compared to the SM one. The distribution functions only enter at the level of computing $\Pi(2\pi f a_0/a)$. For practical purposes, we consider equilibrium distributions in most of section 3 (cf. (19) and (20)), but we emphasize that this assumption is not crucial, and that the generalisation of our results to non-equilibrium situations is straightforward (cf. (21)). In sections 4 and 5, we for simplicity further assume that the SM and hidden sector temperatures are equal to each other.⁴ If the hidden sector temperature deviates from that of the SM, our assumptions imply that their ratio is approximately a model-dependent constant over the domain of integration in equation (15). Hence, the discussion can be generalized to other hidden sector temperatures by an appropriate re-scaling of the production rate Π . Finally, in practice, we consider the contribution from one hidden particle at a time. If there are several hidden particles, the signals are additive in the enhanced regime as long as the total energy density is dominated by the SM.

² The size of the final GWB can be expressed also in terms of the characteristic strain h_c , which is defined as

$$h_c^2 = \frac{3H_0^2}{2\pi^2 f^2} \Omega_{\text{gw}} \propto \frac{h^2 \Omega_{\text{gw}}}{f^2} . \quad (14)$$

³ See appendix D for formulae equivalent to (11) and (15) for more general expansion histories that e.g. deviate from radiation domination.

⁴ To satisfy observational constraints e.g. from big bang nucleosynthesis, thermalized hidden sectors are generically expected to be colder than the SM plasma [48, 49], but it has been argued that larger temperatures can be viable in certain cases [50, 51].

3 Gravitational wave production rates

The GW production rate Π is the final ingredient needed to predict the GWB (15). In this section, we first summarize some existing results for thermal equilibrium production due to the SM and a generic feebly interacting (pseudo-)scalar, and then present the contribution due to a generic feebly interacting fermion. We finally provide compact summary formulae that encompass both the scalar and fermionic cases and are suitable for phenomenological applications.

In the LISA frequency window, and for sufficiently large maximal temperatures, the SM contribution is dominated by hydrodynamic fluctuations of the right-handed leptons [36–38], yielding the production rate [22]

$$\Pi^{\text{SM}} = 8\eta_{\text{SM}}T = \frac{8\pi^2 g_{\text{SM}}}{225} \frac{T^5}{\Upsilon_{\text{SM}}} \approx \frac{16T^4}{g^4 \ln(\frac{5T}{m_D})} \approx 400T^4, \quad m_D^2 = \frac{11}{6} g^2 T^2, \quad (16)$$

where $g \approx 0.36$ is the U(1) hypercharge gauge coupling, m_D the associated Debye mass, and $g_{\text{SM}} = 6$ the degrees of freedom associated with the right-handed leptons. The width Υ_{SM} is defined consistent with our conventions in (26), which simplifies comparing the SM and new physics contributions. Ignoring the running of the weak hypercharge coupling, (16) yields energy density

$$h^2 \Omega_{\text{gw}}^{\text{SM}}(f) \simeq 1.03 \cdot 10^{-36} \times \left(\frac{f}{\text{Hz}} \right)^3 \times \frac{T_{\text{max}}}{m_{\text{Pl}}}, \quad (17)$$

which depends only on T_{max} . For modes that never leave the horizon, this temperature is closely related to the reheating temperature after inflation, and can probe the dynamics of reheating [23, 25]. Given a model of inflation, the CMB is sensitive to the reheating epoch [52–54], and next-generation observatories can potentially independently determine the reheating temperature [55, 56], highlighting the complementarity of multi-messenger probes of the early universe.

3.1 Feebly interacting particles

The production rate due to hydrodynamic fluctuations of a single feebly interacting (pseudo-)scalar is [34, 39]⁵

$$\Pi \simeq \int dp p^6 \frac{4n_B(\epsilon)(1+n_B(\epsilon))}{15\pi^2 \epsilon^2} \frac{1}{2\Upsilon_p} F\left(\frac{k}{2\Upsilon_p}, \frac{p}{\epsilon}\right), \quad F(x, v) = \begin{cases} \frac{1}{1+x^2} & v \ll 1 \\ 1 & v = 1 \wedge x \ll 1 \\ \frac{5}{2x^2} & v = 1 \wedge x \gg 1 \end{cases}, \quad (19)$$

⁵ The complete expression for the function $F(x, v)$ is

$$F(x, v) = \frac{30(4x^2 + 5x^2(1-v^2) - 3)}{48v^4 x^4} + \frac{30x(1-x^2(1-v^2))}{16v^5 x^5} \ln \frac{1+x^2(1+v)^2}{1+x^2(1-v)^2} + \frac{15(1-x^2(1-v^2))^2 - 60x^2}{16v^5 x^5} \arctan \frac{2vx}{1+x^2(1-v^2)}. \quad (18)$$

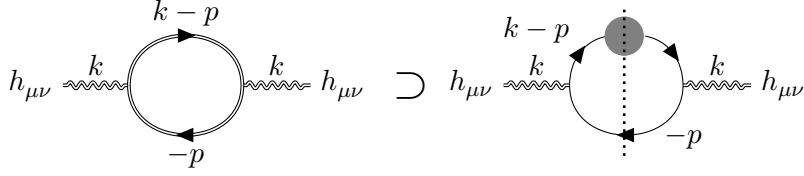


Figure 1: To find the GW production due to a feebly interacting fermion, we compute the resummed Feynman diagram shown on the left-hand side, where the straight double lines represent resummed ψ propagators. Our result encompasses an infinite class of diagrams in fixed-order perturbation theory, including the one depicted on the right-hand side, where the grey blob denotes a single self-energy insertion. The dotted line signaling cut propagators, the optical theorem implies that it and other diagrams we include together encode the rate of producing gravitons as bremsstrahlung.

where Υ_p is the finite temperature width of the new particle, $\epsilon^2 = \mathbf{p}^2 + m^2$ is its energy squared, and $n_B(\epsilon) = [\exp(\beta\epsilon) - 1]^{-1}$ is the usual Bose-Einstein distribution. The corresponding expression for fermions is dominated by the resummed diagram shown in figure 1; it coincides with (19) up to an overall factor $2c_X$ that counts the internal degrees of freedom ($c_X = 1$ for a Majorana fermion and $c_X = 2$ for a Dirac fermion),

$$\Pi(k) \stackrel{k \ll \alpha^2 T}{\simeq} 2c_X \int_0^\infty dp p^6 \frac{4n_F(\epsilon)(1 - n_F(\epsilon))}{15\pi^2 \epsilon^2} \frac{1}{2\Upsilon_p} F\left(\frac{k}{2\Upsilon_p}, \frac{p}{\epsilon}\right), \quad (20)$$

where $F(x, v)$ is defined as in expression (18) and $n_F(\epsilon) = [\exp(\beta\epsilon) + 1]^{-1}$ is the Fermi-Dirac distribution. Although our primary focus is the enhanced regime $x \ll 1$, where $F(x, v) \rightarrow 1$, we note that expression (20) is also a valid approximation of the wave-function type diagram in figure 1 for larger frequencies $\Upsilon_p < k \ll T$. As indicated by the Bose-Einstein and Fermi-Dirac distributions $n_B(p_0)$ and $n_F(p_0)$, the expressions (19) and (20) assume that the hidden sector is in thermal equilibrium. They can be generalised to non-equilibrium expressions in which the distributions are replaced by general phase space distribution functions $n(p_0)$. We present the derivation for the fermionic case in appendix A, finding the result

$$\Pi(k) \simeq \frac{c_X}{2} \int \frac{d^3 \mathbf{p}}{(2\pi)^3} p_\perp^4 [D(\epsilon, \epsilon) + D(-\epsilon, -\epsilon)] \frac{2\Upsilon_p}{k^2(\epsilon - p_\parallel)^2 + 4\epsilon^2 \Upsilon_p^2}, \quad (21)$$

where

$$D(p_0, q_0) = (1 - n(p_0))n(q_0) + n(p_0)(1 - n(q_0)). \quad (22)$$

In thermal equilibrium, one has $D(\epsilon, \epsilon) = 2n_F(\epsilon)(1 - n_F(\epsilon))$. Inserting this expression and evaluating the angular integral, we obtain (20) as a limit of (21).

3.2 Approximate formulae for phenomenology

The production rate (20) is remarkably similar to its (pseudo-)scalar equivalent (19). In the high ($m \ll T$) and low temperature ($m \gg T$) cases, we can combine the two expressions into a

single, approximate formula by replacing the momentum-dependent width Υ_p with its thermal average

$$\Upsilon_{\text{av}} \equiv \frac{1}{2\pi^2 N_{\text{eq}}} \int_0^\infty dp p^2 n_X(\epsilon) \Upsilon_p , \quad N_{\text{eq}} = \frac{1}{2\pi^2} \int_0^\infty dp p^2 n_X(\epsilon) , \quad (23)$$

where $n_X \in \{n_B, n_F\}$ is either the Bose-Einstein or Fermi-Dirac distribution, depending on the spin of the hidden particle. Using Υ_{av} and setting either $v = p/\epsilon \rightarrow 0$ or $v = p/\epsilon \rightarrow 1$, the function $F(x, v)$ becomes momentum-independent and can be pulled out of the integrals in eqs. (19) and (20). In the low-temperature case, it takes on the very simple form

$$F(x, v) \stackrel{v \rightarrow 0}{=} \frac{1}{1 + x^2} , \quad (24)$$

but the high-temperature case is more complicated. For phenomenological applications, we can nevertheless approximate $F(x, v)$ by interpolating the function between $x \ll 1$ and $x \gg 1$, which gives

$$F(x, v) \stackrel{v \rightarrow 1}{\approx} \frac{5}{5 + 2x^2} . \quad (25)$$

We expect this approximation to be worst for $x \approx 1$. Indeed, setting $x = v = 1$, the above expression yields $F(x, v) \approx 0.71$, while the exact expression (18) yields $F(x, v) \approx 0.56$, so that the approximation overestimates the gravitational wave production rate by roughly 30%. However, this is still sufficient for an order of magnitude estimate of the gravitational wave background. In addition, the extremal regimes $x \ll 1$ and $x \gg 1$ are generically expected to be the most relevant for phenomenological applications.

Using Υ_{av} , and pulling out $F(x, v)$, the remaining integrals in (19) and (20) can be computed analytically. For high temperatures, one obtains

$$\Pi(k) \stackrel{m \ll T}{\simeq} g_X \frac{16\pi^2}{225} T^5 \frac{5\Upsilon_{\text{av}}}{k^2 + 10\Upsilon_{\text{av}}^2} , \quad g_X = \begin{cases} 1 & \text{Spin 0} \\ 2 \cdot c_X & \text{Spin } 1/2 \end{cases} , \quad (26)$$

where we have neglected a relative factor of $7/8$ in fermionic case that originates from the distribution functions.

For low temperatures, one has to distinguish between particles that retain a relativistic momentum distribution, e.g. because they undergo relativistic freeze-out at some temperature $T_f \gg m$, and particles whose distribution function becomes non-relativistic. For the relativistic case, one obtains

$$\Pi(k) \stackrel{T \lesssim m \ll T_f}{\simeq} g_X \frac{64\pi^4}{315} \frac{T^7}{m^2} \frac{2\Upsilon_{\text{av}}}{k^2 + 4\Upsilon_{\text{av}}^2} , \quad (27)$$

where we have now neglected a relative factor of $31/32$ in the fermionic case. Note that this rate is independent of the freeze-out temperature. For particles that assume a non-relativistic momentum distribution, freezing out at some temperature $T_f \lesssim m$, one obtains the expression

$$\Pi(k) \stackrel{T, T_f \lesssim m}{\simeq} g_X \left(\frac{2}{\pi}\right)^{3/2} \left[\frac{T^7}{m^2} \left(\frac{\xi m}{T}\right)^{7/2} e^{-\xi m/T} \right] \frac{2\Upsilon_{\text{av}}}{k^2 + 4\Upsilon_{\text{av}}^2} , \quad \xi = \begin{cases} 1 & T > T_f \\ T/T_f & T < T_f \end{cases} , \quad (28)$$

which explicitly depends on T_f . Setting $T_f \rightarrow 0$, this expression also captures particles that never freeze-out but always remain in thermal equilibrium. This is the case e.g. for unstable particles with a large width $\Upsilon_{\text{av}} > H$, which remain in thermal equilibrium as they decay. In contrast, we expect that unstable particles with a *small* width $\Upsilon_{\text{av}} \ll H$ are better captured by the relativistic formula (27), because the explicit $\propto T^7/k^2 \sim T^5$ suppression in (27) effectively cuts off GW production well before decays can significantly impact their momentum distribution and number density.

Finally, we note that the rate for a relativistic distribution is strictly larger than the one for a non-relativistic distribution, so that it can be used to obtain a model-independent upper bound on GW production, cf. section 4.2.

4 Phenomenology

In this section, we apply the results of section 3 to study the phenomenology and the prospects of detecting GWBs produced by feebly interacting particles. The full background can be computed by numerically integrating the production rates in (19) and (20). To help illustrate its qualitative features, we also derive analytical expressions that are applicable in various GW production regimes.

4.1 Generic features

The GW production rate is proportional to $k^3 \Pi(k)$. In thermal equilibrium, it depends on the physical graviton momentum $k = 2\pi f a_0/a$, the temperature of the early universe plasma T , and the properties of the particles driving production. The SM contribution (16) is determined by the width Υ_{SM} , which measures the free-streaming length of the right-handed SM leptons. Likewise, the new physics contributions (19) and (20) due a single feebly interacting particle mainly depend on its mass m and the width Υ_{av} , which characterizes the free-streaming length of the new particle.

The new physics contribution dominates the SM contribution in the regime $k < \Upsilon_{\text{av}} \ll \Upsilon_{\text{SM}}$. In this regime, hydrodynamics governs both sectors. The new physics contribution (20) scales as k^3/Υ_{av} while the smaller SM contribution (16) scales as k^3/Υ_{SM} , so that both contributions grow like k^3 . For larger momenta $\Upsilon_{\text{av}} < k < \Upsilon_{\text{SM}}$, hydrodynamics still governs the SM but not the hidden sector. It is no longer necessary to resum wave-function type corrections to the hidden particle propagators, so that a more Boltzmann-like picture of the hidden sector as a particle gas becomes appropriate. The new physics contribution now scales as $k\Upsilon_{\text{av}}$, growing like k . Since the SM contribution continues to grow like k^3 , it eventually overtakes the hidden sector to dominate the overall production rate. For even larger momenta $\Upsilon_{\text{SM}} < k$, the Boltzmann picture captures both the SM and the hidden sector. The overall production rate still grows and finally peaks at momenta $k \sim \pi T$. Beyond this peak, the production rate is Boltzmann-suppressed and therefore effectively cut off.

The most important parameter determining the magnitude of the final background is the maximal temperature T_\star of the hidden sector plasma, which is a highly model dependent and encodes e.g. the specific dynamics of reheating. Although we assume that the SM and hidden sector plasmas share the same temperature T , it is possible for the SM to thermalize well before

or after the hidden sector, leading to different effective values of T_\star for the two contributions. Along this line of reasoning, one might worry that it is impossible to produce a sufficient quantity of thermally distributed feebly interacting hidden particles early enough to result in a significant contribution in the final GWB. However, if the SM is produced before the hidden sector, the SM can produce thermalized hidden particles via freeze-in, which puts an effective lower bound on T_\star . Explicitly, interactions between the SM and hidden sectors equilibrate for temperatures $\Upsilon_{\text{av}} \sim H \propto T^2/m_{\text{Pl}}$. One way to evade this worst-case scenario, which can still result in a significant new physics contribution to the final GWB, is to produce the hidden sector either via non-renormalizeable interactions (cf. section 4.3.2) or non-thermally, e.g. via (p)reheating or the decay of heavy new particles.

Focusing on a fixed frequency f , the production rate changes over time as the temperature of the early universe plasma decreases. Since the physical momentum $k \propto f/a$ redshifts the same as the temperature $T \propto 1/a$, the ratio k/T remains approximately constant, and the peak of the production rate at $k \sim \pi T$ translates into the same temperature-independent frequency

$$f_{\text{peak}} \equiv \frac{T_0}{2} \left[\frac{g_s(T_0)}{g_s(T)} \right]^{1/3} \approx 6 \cdot 10^{10} \text{ Hz} , \quad (29)$$

which approximately determines the peak frequency of the final GWB. In the following, our primary focus is on the phenomenology of direct detection experiments, which are typically sensitive to much lower frequencies with redshifted momenta $k \ll T$. These modes can be outside the causal horizon ($k < H$) at the onset of GW production. Since super-horizon modes of tensor perturbations are static (cf. e.g. section 5.4 in [57]), production of these modes is delayed until they re-enter the horizon. Adopting the same standard cosmology as in section 2.2, a given mode with frequency f re-enters the horizon at the entry temperature

$$T_{\text{entry}}(f) = m_0 \frac{\pi f}{f_{\text{peak}}} , \quad H(T = T_{\text{entry}}) = k . \quad (30)$$

Modes with $T_{\text{entry}} > T_\star$ enter the horizon before GW production begins, causing no delay, while modes with $T_{\text{entry}} < T_\star$ start to be produced only upon re-entry, so that one has to replace $T_\star \rightarrow T_{\text{entry}}$ in the integral (15). Hence, the maximal temperature T_{max} is

$$T_{\text{max}} = \min(T_{\text{entry}}, T_\star) = \frac{\min(f, f_\star)}{f_\star} T_\star \simeq \frac{f}{f + f_\star} T_\star , \quad (31)$$

where the horizon frequency f_\star is the largest frequency for which production is delayed by the causal horizon,

$$f_\star = \frac{f_{\text{peak}}}{\pi} \frac{T_\star}{m_0} \approx 3 \cdot 10^{11} \text{ Hz} \frac{T_\star}{m_{\text{Pl}}} , \quad T_{\text{entry}}(f_\star) = T_\star . \quad (32)$$

For sufficiently small frequencies, the entry temperature can drop below the mass of the hidden particle, $T_{\text{entry}} < m$, so that GW production is restricted to the non-relativistic regime. The frequency at which this happens is the non-relativistic frequency

$$f_{\text{nr}} = \frac{f_{\text{peak}}}{\pi} \frac{m}{m_0} \approx 3 \cdot 10^{11} \text{ Hz} \frac{m}{m_{\text{Pl}}} , \quad T_{\text{entry}}(f_{\text{nr}}) = m . \quad (33)$$

In principle, the entry temperature can even drop below the minimal temperature T_{\min} . However, this effect is less relevant, since we generically expect to be able to consider minimal temperatures e.g. in the TeV range or even lower. In this case, the frequency for which T_{entry} drops below T_{\min} is less than 10^{-6} Hz and therefore well below the regime of phenomenological interest.

In the regime $f \ll f_{\text{peak}}$ (or equivalently $k \ll T$), GW production is governed by the phenomenological formulae we derived in section 3.2. At high temperatures $T \gg m$, the new physics contribution to the relevant production rate is independent of the mass m and can be approximated using the phenomenological expression (26). Once the temperature falls below the mass, $T \lesssim m$, one has to distinguish between particles that retain their relativistic momentum distribution, e.g. due to relativistic freeze-out, and particles which assume a non-relativistic distribution. If the hidden particle remains in thermal equilibrium with the SM plasma, its contribution to the production rate becomes Boltzmann suppressed and becomes effectively irrelevant. However, if the particle freezes-out or if it is unstable but long lived, with a width $\Upsilon_{\text{av}} \ll H$, GW production can continue in the low temperature regime $T < m$ for some time. The phenomenological expression (27) captures low-temperature production in case of a relativistic freeze-out, while expression (28) captures the case of a non-relativistic freeze-out.

4.2 Model-independent upper bound

The phenomenological formulae (26) and (27) imply an upper bound on the GWB for frequencies $f \ll f_{\text{peak}}$ that is saturated at the transition between the hydrodynamic and Boltzmann regimes. Explicitly, the high- and low temperature expressions (26) and (27) are maximal for widths

$$\Upsilon_{\text{av}} = \begin{cases} k/\sqrt{10} & T > m \\ k/2 & T < m \end{cases}. \quad (34)$$

Inserting these values into the formulae (26) and (27), one obtains two separate bounds on the high-temperature contribution,

$$h^2 \Omega_{\text{gw}}^{T>m}(f) < 2.6 \cdot 10^{-29} \times \left(\frac{f}{\text{Hz}}\right)^2 \times g_X \frac{\max(T_{\text{max}}, m) - \max(T_{\min}, m)}{m_{\text{Pl}}}, \quad (35)$$

and the low temperature contribution,

$$h^2 \Omega_{\text{gw}}^{T<m}(f) < 1.6 \cdot 10^{-28} \times \left(\frac{f}{\text{Hz}}\right)^2 \times g_X \frac{\min(T_{\text{max}}^3, m^3) - \min(T_{\min}^3, m^3)}{m^2 m_{\text{Pl}}}, \quad (36)$$

to the final gravitational wave energy density. Maximizing the sum of both contributions, we set $T_{\min} \rightarrow 0$ and $m \rightarrow T_{\text{max}}$. Inserting expression (31), this gives

$$h^2 \Omega_{\text{gw}}(f) < 4.9 \cdot 10^{-40} \times g_X \left(\frac{f}{\text{Hz}}\right)^2 \min\left(\frac{f}{\text{Hz}}, \frac{f_\star}{\text{Hz}}\right). \quad (37)$$

This expression depends only on g_X and T_\star . We can eliminate the T_\star dependence by using that $\min(f, f_\star) < f$, finding the slightly weaker bound

$$h^2 \Omega_{\text{gw}}(f) < 4.9 \cdot 10^{-40} \times g_X \left(\frac{f}{\text{Hz}}\right)^3, \quad (38)$$

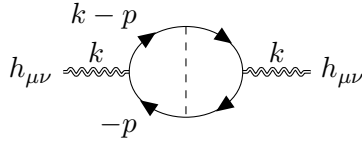


Figure 2: Example of a vertex-type correction to the rate of GW production from feebly interacting fermions.

where g_X is now the only remaining model-dependent parameter. On the other hand, considering feebly interacting particles with a given mass m , and focusing on frequencies $f < f_{\text{nr}}$, so that GW production is delayed until the particle is non-relativistic, we obtain the much more stringent bound

$$h^2 \Omega_{\text{gw}}(f) \stackrel{f < f_{\text{nr}}}{<} 4.9 \cdot 10^{-40} \times g_X \left(\frac{f}{\text{Hz}} \right)^3 \frac{f^2}{f_{\text{nr}}^2} . \quad (39)$$

The $h^2 \Omega_{\text{gw}} \propto f^5$ scaling of this bound shows that the final GW spectrum is effectively cut off below $f = f_{\text{nr}}$. If we require e.g. $f_{\text{nr}} < 10^{-1} \text{ Hz}$, such that the entire region of phenomenological interest lies above this cut-off, one finds that the mass of the feebly interacting particle responsible for GW production should be $m < 1.1 \cdot 10^8 \text{ GeV}$.

These bounds, of course, rely on a number of implicit assumptions. For example, we have not included contributions to the production rate generated by vertex-type diagrams such as the one shown in figure 2 or higher order diagrams. However, we expect that including such diagrams will at most yield an order one correction to the overall GW production rate and should not significantly modify the bounds. We also assumed that no entropy is transferred from the SM to the hidden sector. If the SM plasma can dump a significant amount of entropy into the hidden sector, this would cause the GWB to be diluted less than in standard cosmology and therefore enhance it. Of course, it is also possible to transfer entropy from the hidden sector to the SM plasma, but this does not impact the validity of our bounds, since it would simply enhance the dilution of the GWB.

Finally, the bounds (35) and (36) only apply to GWs emitted by thermal equilibrium fluctuations of the early universe plasma. They explicitly do not apply to GWBs from out-of-equilibrium processes with very different underlying physics, such as strong first order phase transitions, production during (cold) inflation, or turbulence during preheating (cf. [19]). For example, a number of recent works have found that particle decays during reheating can produce a background significantly in excess of these upper bounds [58–61]. However, these works seem to compute the GW production rate without accounting for the resummation of wave-function type corrections that is necessary in the hydrodynamic regime. We expect that systematically incorporating these effects, using e.g. the approach we have employed in section 3, which results in an expression for the production rate (20) that can already accommodate out-of-equilibrium distribution functions, would yield a significant suppression of the resulting GWB.

4.3 Analytic estimates of the high-temperature background

The width Υ_{av} determines the more detailed features of the spectrum. It generically becomes smaller as the temperatures decreases and depends on the mass of the hidden particle m , the temperature T , any number of coupling constants, and potentially some heavy new physics scale $\Lambda \gg m, T$. If the width is dominated by interactions with the same mass dimension d , and neglecting the temperature dependence of running couplings, it is expected to scale as

$$\Upsilon_{\text{av}} \simeq y T \left(\frac{T}{\Lambda} \right)^{2(d-4)} \begin{cases} 1 & T \gg m \\ (m/T)^n & T \lesssim m \end{cases}, \quad n \leq 1 + 2(d-4), \quad (40)$$

where y is some combination of coupling constants and other dimensionless parameters. The integer n depends on the properties of the hidden particle and its interactions. For an unstable particle, the width becomes temperature independent for $T \rightarrow 0$, so that $n = 1 + 2(d-4)$, but if the particle is stable n is a model-dependent parameter. If the low-temperature width is dominated by $2 \leftrightarrow 2$ scattering events involving relativistic particles in the plasma, it is related to the thermal average of the total scattering cross section [62],

$$\Upsilon_{\text{av}} \propto \langle v_{\text{rel}} \sigma \rangle N, \quad (41)$$

where σ is the relevant scattering cross-section, v_{rel} the relative velocity of the two scattering particles, and N the number density of the scattering partner (for SM particles this is just $N \sim T^3$).⁶

In the remainder of this section, we assume that $m \ll T_*$ and focus on frequencies $f > f_{\text{nr}}$. In this case, one has $m \ll T_{\text{max}}$, and we expect production at high temperatures ($m \ll T$) to dominate the overall GWB. Using the largely model-independent temperature scaling of Υ_{av} at these temperatures, we can derive generic analytic approximations for the resulting GWB. However, we caution that, in principle, one also has to account for the non-relativistic contribution from temperatures $T < m$, which has to be evaluated on a case-by-case basis.

4.3.1 Renormalizable interactions

If the width is dominated by renormalizable interactions with $d = 4$, the physical momentum k redshifts in the same way as the high-temperature width Υ_{av} . The ratio Υ_{av}/k is then fixed for a given frequency f , and the relativistic contribution to the background is always either in the Boltzmann (for $f \gg f_c$), hydrodynamic ($f \ll f_c$), or intermediate regime (for $f \sim f_c$). The production rate saturates the upper bound (35) at the critical frequency f_c , which is the frequency at which the associated, redshifted graviton momentum satisfies condition (34),

$$k = \sqrt{10} \Upsilon_{\text{av}} \quad \Leftrightarrow \quad f = f_c, \quad \frac{f_c}{y} \equiv \frac{\sqrt{10}}{\pi} f_{\text{peak}} \simeq 6 \cdot 10^{10} \text{ Hz}. \quad (42)$$

The effective coupling y is a combination of coupling constants and other model parameters. Employing the same general assumptions as in section 2.2, it is the only remaining model-dependent quantity, and the critical frequency f_c directly probes its size. If one requires e.g.

⁶ Note that the feebly interacting particle does not have to interact with the SM at all, as the width Υ_{av} can arise solely from interactions within the hidden sector.

$f_c \sim 1 \text{ Hz}$, so that the GWB is maximal in the frequency window of the next-generation of laser interferometers, this gives an optimal coupling parameter $y \sim 1.7 \cdot 10^{-11}$.

We estimate the high-temperature background by inserting the average width (40) into the relativistic GW production rate (26) in order to compute the integral in (15). For $f > f_{\text{nr}}$, this yields

$$h^2 \Omega_{\text{gw}}^{T>m}(f) \stackrel{d=4}{\simeq} 1.6 \cdot 10^{-40} \times g_X \frac{f f_c}{f_c^2 + f^2} \left(\frac{f}{\text{Hz}} \right)^2 \min\left(\frac{f}{\text{Hz}}, \frac{f_\star}{\text{Hz}} \right). \quad (43)$$

As it should, this expression saturates the bound (35) for $f = f_c$. T_\star is the earliest temperature at which hidden sector thermal fluctuations begin to produce GWs and, in principle, a free parameter. As mentioned above, the hidden sector can thermalize well before or after the SM, so that T_\star may be significantly lower than the maximal temperature of the SM plasma after reheating. However, the same processes that give rise to $\Upsilon_{\text{av}} \sim yT$ can also produce hidden particles via thermal freeze-in, which puts an effective lower bound on T_\star . This production mode equilibrates when $\Upsilon_{\text{av}} > H = T^2/m_0$, which gives $T_\star > y m_0$ (or equivalently $\sqrt{10} f_\star > f_c$) as the temperature where freeze-in production alone starts to be sufficient to thermalize the hidden sector.

Expression (43) is generic and also captures the SM contribution to the final GWB. Comparing the production rate (16) with the width parametrization (40), we find the critical frequency

$$f_c^{\text{SM}} \approx 3.1 \cdot 10^8 \text{ Hz}. \quad (44)$$

This implies that (16), which is accurate in the hydrodynamic limit, is not expected to be valid for frequencies above 10^8 Hz . For smaller frequencies, and using $g_X = g_{\text{SM}} = 6$, we find the SM background

$$h^2 \Omega_{\text{gw}}^{\text{SM}}(f) \stackrel{f < f_c^{\text{SM}}}{\simeq} 3.2 \cdot 10^{-48} \times \left(\frac{f}{\text{Hz}} \right)^3 \min\left(\frac{f}{\text{Hz}}, \frac{f_\star}{\text{Hz}} \right). \quad (45)$$

While this background was already estimated in [22, 23, 25], these references neglect that GW emission is suppressed for super-horizon modes, delaying GW production until after horizon re-entry. We phenomenologically incorporate this effect by rescaling the maximal temperature according to equation (31).

4.3.2 Non-renormalizable interactions

One way to enhance the production of the hidden particles at high temperatures is to include non-renormalizable interactions with $d > 4$, which are more efficient at high temperature. These interactions contribute to and potentially dominate the width in equation (40), resulting in more complicated temperature dependence compared to the renormalizable case. In this case, the ratio Υ_{av}/k also depends on temperature, so that a given GW frequency f can receive contributions from several different production regimes.

Figure 3 illustrates the interplay between these regimes and the horizon entry temperature, leading to a variety of GW spectra. As the universe expands and cools down, the width generically decreases faster than the momentum, so that a GW mode that is initially produced

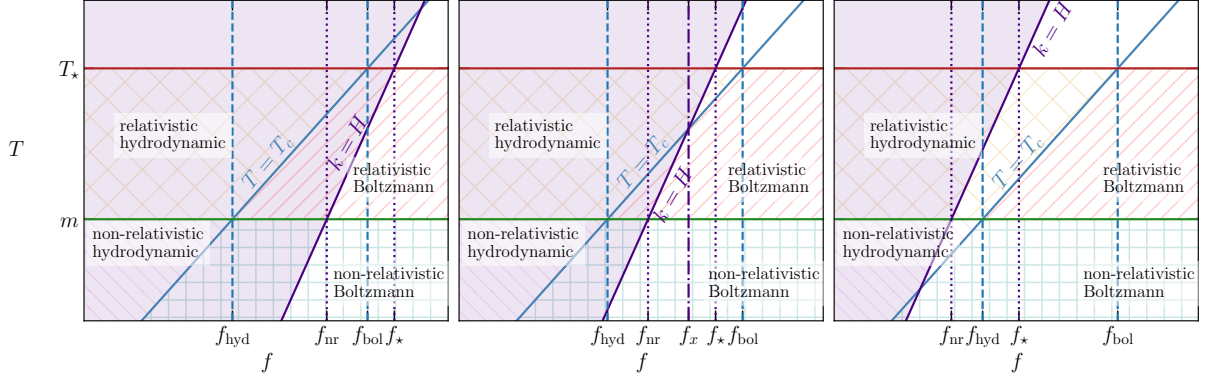


Figure 3: Cases of GW production for a width Υ_{av} dominated by non-renormalizable interactions. At each temperature, modes are produced either in the hydrodynamic ($k < \Upsilon_{\text{av}}$) or Boltzmann ($k > \Upsilon_{\text{av}}$) regime. They transition from the hydrodynamic to the Boltzmann regime as the temperature drops below their respective critical temperature T_c . Modes with $f > f_{\text{bol}}$ are only produced in the Boltzmann regime while modes with $f < f_{\text{hyd}}$ are only produced in the hydrodynamic regime. The purple shading shows that GW production is suppressed because modes are outside the horizon. Modes with $f > f_*$ are not affected by the horizon, while modes with $f < f_{\text{nr}}$ enter it only after the hidden particle becomes non-relativistic. For $T < m$, the transition between the hydrodynamic and Boltzmann regimes becomes more model-dependent, the line shown in the figure corresponds to $n = 0$ from eq. (40).

in the hydrodynamic regime can later transition to the Boltzmann regime. For a given frequency f , and using the high-temperature scaling of the width Υ_{av} in (40), this transition occurs at the critical temperature

$$T_c(f) = \Lambda \left(\frac{f}{f_c} \right)^{1/2(d-4)}, \quad (46)$$

where f_c is the same critical frequency as in equation (42). The critical temperature increases with frequency and is equal to the cutoff scale Λ for $f = f_c$. Each other mass scale defines its own characteristic frequency as the frequency for which T_c is equal to the mass scale. In particular, the maximal temperature T_* corresponds to the Boltzmann frequency

$$f_{\text{bol}} \equiv f_c \left(\frac{T_*}{\Lambda} \right)^{2(d-4)}, \quad T_c(f_{\text{bol}}) = T_*. \quad (47)$$

Above this frequency, T_c is larger than T_* , and the high-temperature background is produced entirely in the Boltzmann regime. If the hidden particle is massive, its mass m likewise corresponds to the hydrodynamic frequency

$$f_{\text{hyd}} \equiv f_c \left(\frac{m}{\Lambda} \right)^{2(d-4)}, \quad T_c(f_{\text{hyd}}) = m. \quad (48)$$

Below this frequency, T_c is smaller than m , and the high-temperature background is produced entirely in the hydrodynamic regime.

Since we focus on the case $m \ll T_*$, and since $m \ll \Lambda$ is necessary for a consistent effective field theory (EFT) description, f_{hyd} has to be much smaller than both f_{bol} and f_c . Naively, one

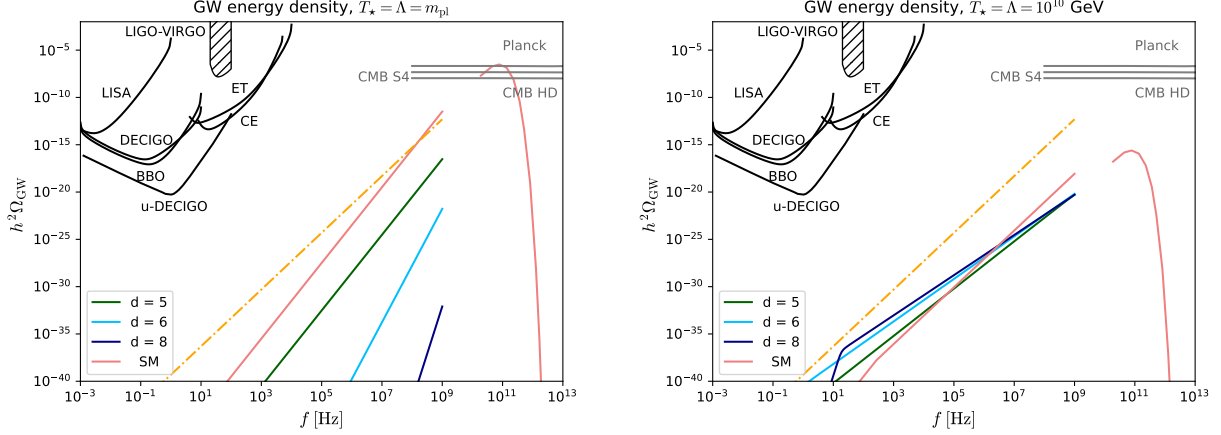


Figure 4: Estimate of the GW background from non-renormalizable interactions with dimension $d > 4$ for $T_\star = \Lambda = m_{\text{Pl}}$ (Left) and $T_\star = \Lambda = 10^{10} \text{ GeV}$ (Right), cf. equations (50) to (52). The dashed orange line shows the upper bound (38) and the red line shows the SM background resulting from the same value of T_\star . The SM line has been computed using the production rate from [22] while accounting for previously missed super-horizon effects, see also the last paragraph in section 4.3.1. Although it appears to violate the upper bound, which does in principle apply to the SM contribution, this occurs above the frequency (44), where the validity of (45) is questionable. For much larger frequencies (beyond the visible gap) one enters the peak region, where vertex-type and other diagrams should be included. This possibly also explains the apparent slight mismatch between the two parts of the curve. In both plots, we consider a hidden particle mass $m = 0$ and coupling parameter $y = 1$, cf. equation (40). The signal can be enhanced and/or present additional features at low frequencies if $y \ll 1$, cf. e.g. figure 5. The smooth black lines are extracted from [63, 64] and show experimental power-law integrated sensitivities [65] of various prospective laser interferometers. The black hatched region highlights the already excluded parameter space from the third observing run of LIGO and VIRGO [66]. Finally, the grey lines show the sensitivity of Planck [67] and its proposed successors, CMB-S4 [68] and CMB-HD [69].

might assume that the EFT setup also requires $T_\star \ll \Lambda$, and therefore $f_{\text{bol}} \ll f_c$, but this is not entirely true. Considering larger maximal temperatures, the setup can be salvaged for modes with frequency $f < f_c$, where T_c is smaller than Λ . For temperatures $T_c < T < \Lambda$, these modes are first produced in the hydrodynamic regime. Since $d > 4$, the resulting GW production rate increases as the temperature decreases, so that the GWB contribution at $T \sim T_c$, where production transitions into the Boltzmann regime, is more important than the contribution generated at temperatures $T \gtrsim \Lambda$, where the EFT description breaks down. Unfortunately, the same reasoning does not extend to frequencies $f > f_c$, which, at temperatures suitable for the EFT description, are only produced in the Boltzmann regime. Since the GW production rate in the Boltzmann regime becomes smaller as the temperature decreases, the final background is dominated by the contribution generated at the largest available temperature, i.e. T_{max} . Hence, and in line with the naive expectation for $T_{\text{max}} > \Lambda$, the EFT description cannot be used to determine the size of the overall background at these frequencies.

At intermediate frequencies $f_{\text{hyd}} < f < f_{\text{bol}}$, the high-temperature background can be produced both in the hydrodynamic and Boltzmann regime, based on the precise relationship

between T_c and T_{entry} . Both characteristic temperatures are functions of f and equal to each other at the crossing frequency

$$f_x \equiv f_c \left(\frac{f_{\text{peak}} \Lambda}{\pi f_c m_0} \right)^{1 + \frac{1}{2(d-4)-1}}, \quad T_c(f_x) = T_{\text{entry}}(f_x). \quad (49)$$

The ordering of the characteristic frequencies f_x , f_{hyd} , and f_{bol} determines the spectrum of the final GWB. Following the derivation outlined in appendix C, we find three physically distinct spectra:

1. If $f_{\text{bol}} < f_x$, the horizon entry temperature is always smaller than the critical temperature. Hence, GW production is always in the Boltzmann regime, as shown in the left panel of figure 3. The resulting spectrum has two knees, one at f_* , and another one at f_{nr} . The high-temperature contribution to the GWB is

$$h^2 \Omega_{\text{gw}}^{T>m}(f) \stackrel{f_x > f_{\text{bol}}}{\simeq} g_X \frac{1.6 \cdot 10^{-40}}{2(d-4)+1} \left(\frac{f}{\text{Hz}} \right)^2 \frac{f_{\text{bol}}}{\text{Hz}} \begin{cases} 0 & \text{for } f < f_{\text{nr}}, \\ \left(\frac{f}{f_*} \right)^{2(d-4)} & \text{for } f_{\text{nr}} < f < f_*, \\ \frac{f_*}{f} & \text{for } f_* < f. \end{cases} \quad (50)$$

The background produced at lower temperatures $T < m$ contribution is highly suppressed and bounded by the general upper bound (39).

2. If $f_{\text{hyd}} < f_x < f_{\text{bol}}$, the high-temperature background receives contributions from both the Boltzmann and hydrodynamic regimes. High frequencies $f > f_{\text{bol}}$ are produced in the Boltzmann regime and directly probe T_* . Intermediate frequencies $f_x < f < f_{\text{bol}}$ are produced in both regimes, since their critical temperature is smaller than the horizon entry temperature. Since the critical temperature falls below the horizon entry temperature for lower frequencies $f < f_x$, these again only receive contributions from the Boltzmann regime. Hence, the high-temperature contribution to the GWB is

$$h^2 \Omega_{\text{gw}}^{T>m}(f) \stackrel{f_* \gg f_{\text{bol}}}{\simeq} g_X \frac{1.6 \cdot 10^{-40}}{2(d-4)+1} \left(\frac{f}{\text{Hz}} \right)^2 \frac{f_{\text{bol}}}{\text{Hz}} \begin{cases} 0 & \text{for } f < f_{\text{nr}}, \\ \left(\frac{f}{f_*} \right)^{2(d-4)} & \text{for } f_{\text{nr}} < f < f_x, \\ \beta \frac{f_x}{f_{\text{bol}}} \left(\frac{f}{f_x} \right)^{1/2(d-4)} & \text{for } f_x < f < f_{\text{bol}}, \\ \frac{f_*}{f} & \text{for } f_{\text{bol}} < f. \end{cases} \quad (51)$$

This expression coincides with equation (50), except in the range $f_x < f < f_{\text{bol}}$ that also receives a contribution from the hydrodynamic regime. The numerical factor $1 \lesssim \beta \leq 4$ arises due to the integration over $T > T_c$.

3. Finally, if $f_x < f_{\text{hyd}}$, the effects of the horizon can be almost completely neglected, leading to a GWB with one knee at $f = f_*$, one at $f = f_{\text{hyd}}$, and a final one at f_{nr} . The high-temperature contribution to the GWB is

$$h^2 \Omega_{\text{gw}}^{T>m}(f) \stackrel{f_{\text{bol}} \gg f_*, f_{\text{hyd}} \gg f_{\text{nr}}}{\simeq} g_X \frac{1.6 \cdot 10^{-40}}{2(d-4)+1} \left(\frac{f}{\text{Hz}} \right)^2 \frac{f_{\text{bol}}}{\text{Hz}} \begin{cases} 0 & \text{for } f < f_{\text{hyd}}, \\ \beta \frac{f_x}{f_{\text{bol}}} \left(\frac{f}{f_x} \right)^{1/2(d-4)} & \text{for } f_{\text{hyd}} < f < f_{\text{bol}}, \\ \frac{f_*}{f} & \text{for } f_{\text{bol}} < f. \end{cases} \quad (52)$$

Figure 4 shows the GWB arising from a hidden particle whose width is dominated by non-renormalizable interactions in comparison to the sensitivities of various prospective GW detectors. Focusing on the most optimistic scenario, we choose $\Lambda = T_\star$ and consider the two choices for the reheating temperature $T_\star = m_{\text{Pl}}$ and $T_\star = 10^{10}$ GeV. As benchmarks, we set $y = 1$ and consider operators of dimensions 5, 6 and 8. While choosing smaller values for the coupling y might enhance the signal, in general, virtual graviton exchanges constitute an unavoidable contribution to the feebly interacting particles' width and effectively lead to a lower bound on the value of y . Conservatively, i.e. neglecting any quantum gravity effects at the Planck scale, we expect that this should contribute to the width at the very least at dimension 8, such that $y \sim \mathcal{O}(1)$ for $d \gtrsim 8$, which is the value we consider in the figure.

The plot illustrates the frequency dependence of the signal in line with the estimates in equations (50) to (52). For our choice of benchmarks, $f_{\text{bol}} \approx 6 \cdot 10^{10}$ Hz lies above the range of validity of our approximation. For the first benchmark with $T_\star = m_{\text{Pl}}$, one has $f_\star \approx 3 \cdot 10^{11}$ Hz. Hence, $f < f_{\text{bol}} < f_x$ in our region of interest, and the GW signal is captured by equation (50). As expected, the GWB in this scenario scales as $f^{2(d-3)}$ for all frequencies. The fact that $f < f_\star$ also explains why the GWB is suppressed compared to our second scenario $T_\star = 10^{10}$ GeV. Indeed, while $T_\star = m_{\text{Pl}}$, the maximal temperature T_{max} for which GWs can be produced is much lower than the Planck scale and, given that GWs are always produced in the Boltzmann regime, GW production is suppressed by $(T_{\text{entry}}/\Lambda)^{2(d-4)}$. The second benchmark $T_\star = 10^{10}$ GeV presents more interesting features. In that case, one has $f_\star < f_{\text{bol}} < f_x$. For $d = 8$, we observe that the crossing frequency f_x lies in the LISA frequency band. Hence, the GWB scales as $f^{2(d-3)}$ for $f \lesssim 100$ Hz and $f^{2+1/(2(d-4))}$ for larger frequencies, as expected from eq. (51). A similar feature is present for $d = 5$ and $d = 6$ but f_x is pushed towards smaller frequencies. Therefore, a measurement of the slope of the GWB can be used, in principle, to deduce the mass-dimension of the interaction generating the width Υ_{av} . Moreover, depending on the value of T_\star , it is in theory possible to measure the values of all the characteristic frequencies f_{nr} , f_{hyd} , f_x , f_{bol} and f_\star by looking at variations in the slope of the GWB. This way, one may be able to extract information on the mass of the particle as well as the ultraviolet (UV) scale Λ and reheating temperature T_\star .

5 Explicit examples

In the following we illustrate our results for two popular extensions of the SM, namely axion-like particles (ALP) and heavy neutral leptons (HNL).

5.1 Axion-like particles

First appearing as a solution to the strong CP-problem [70–73] (for a review see e.g. [74])⁷ axions and, more generically, ALPs, are also viable dark matter candidates [76–78] (for a review see e.g. [79]), and can drive inflation [80], including realistic warm inflation scenarios [81,

⁷ It has recently been pointed out that the phases from instanton effects and from the mass term are systematically aligned if one reverses the order of the sum over topological sectors and the infinite volume limit, i.e., if these limits are taken the other way around, there is no physical phase, suggesting that there is actually no strong CP problem [75].

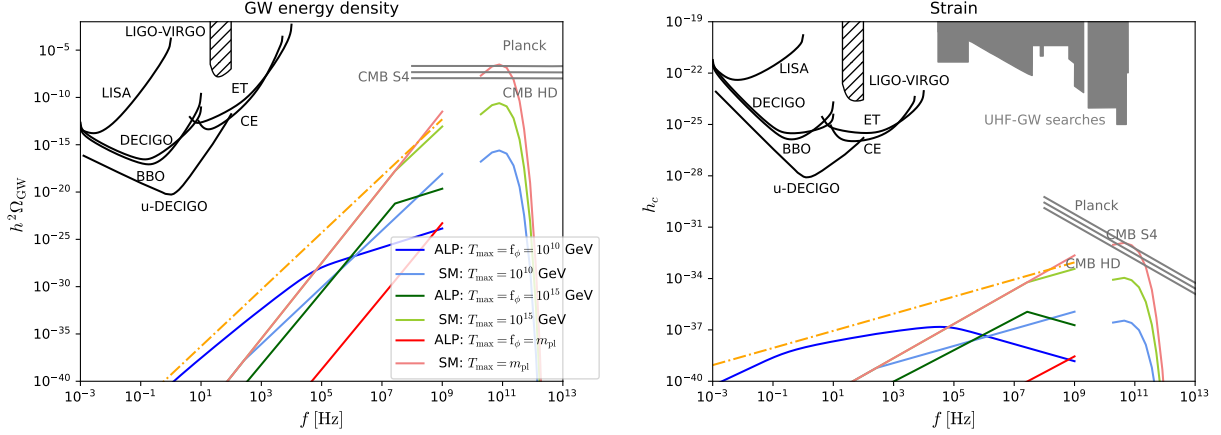


Figure 5: GWB due to thermal fluctuations of a massless ALP with axion decay constants $f_\phi \in \{10^{10}\text{GeV}, 10^{15}\text{GeV}, m_{\text{Pl}}\}$, as measured by the energy density $h^2\Omega_{\text{gw}}$ (Left) or strain h_c (Right). For each line, we choose $T_\star = f_\phi$ and $\Lambda_{\text{IR}} \approx 200\text{ MeV}$, considering QCD-like gauge field. The corresponding SM background for the same reheating temperature T_\star is shown in a lighter version of the same color (blue, green and red respectively). The orange dashed line shows the upper bound (38) (for $g_X = 1$). For details about the SM line and the various experimental constraints in the LISA frequency band, see the caption below figure 4. Additionally, we display in the right plot the sensitivity estimate of some recently proposed searches⁸ for high-frequency GWs [15, 25, 88–93] (cf. also [94]).

82]. As a result, ALPs have become one of the most popular extension of the SM and are currently searched for at a wide range of different experiments [29, 79, 83–86] and astrophysical environments [29, 87].

While the GWB from ALPs was considered within the SMASH [95] model in [25], only the impact on the reheating temperature⁹ T_\star was accounted for; the enhancement due to the feebly-interacting nature of ALPs as well as the suppression coming from the requirement for modes to remain sub-horizon were missed.

In gauge theories, ALPs are generically expected to couple to the topological charge density of the gauge sector,

$$\mathcal{L} \supset \frac{1}{2}(\partial_\mu \phi \partial^\mu \phi - m^2 \phi^2) - \frac{\phi \chi}{f_\phi}, \quad \chi = \frac{\alpha}{16\pi} \tilde{G}_{\mu\nu} G^{\mu\nu}, \quad (53)$$

where ϕ is the axion-like particle, $G_{\mu\nu}$ the gauge field strength tensor, and f_ϕ the axion decay constant. In a minimal setup, $G_{\mu\nu}$ can be e.g. identified with the SM gluon field strength tensor, but one may also consider theories with hidden gauge fields that are not as strongly constrained by SM observations. In the following, we primarily focus on the case of very light ALPs, with mass $m \ll T$. In this case, non-perturbative effects are important for an accurate

⁸We caution that these searches rely on different sets of assumptions, *e.g.* about the strength of the cosmic magnetic fields, and show different levels of maturity. Hence, the gray region might have to be slightly adapted in the future.

⁹Some of the most studied axion production mechanisms, cf. e.g. the misalignment mechanism [76–78], are non-thermal, such that T_\star effectively corresponds more to a thermalization temperature than the reheating temperature.

estimate of the width Υ_{av} . For an asymptotically free theory, one obtains [96]

$$\Upsilon_{\text{av}} \stackrel{m \ll T}{\approx} \kappa n_c^3 (n_c^2 - 1) \frac{\alpha^5 T^3}{f_\phi^2}, \quad \kappa \approx 1.5, \quad \frac{1}{\alpha} \approx \frac{22n_c}{12\pi} \ln\left(\frac{2\pi T}{\Lambda_{\text{IR}}}\right), \quad (54)$$

where n_c is the number of colours associated with the gauge fields and Λ_{IR} the infrared confinement scale at which the gauge coupling α exhibits a Landau pole. In contrast to the generic discussion in section 4.3, we here also account for the running of α . For $n_c = 3$, one finds

$$f_{\text{bol}} \approx \left(\frac{T_\star}{f_\phi}\right)^2 \left(\frac{\alpha(T_\star)}{0.02}\right)^5 \times 6 \cdot 10^4 \text{ Hz}. \quad (55)$$

f_x can be obtained numerically but does not have an analytical expression. Indeed, the logarithmic temperature dependence of the coupling α is not captured by eq. (40) rendering the approximation (49) inadequate.

Figure 5 shows the GWB predicted by the approximate formula (26) for various values of f_ϕ . We show the results for both the GW energy density fraction Ω_{gw} per logarithmic wave number interval and the characteristic strain (14). The reheating temperature T_\star is, in principle, an independent parameter. We consider the case $T_\star = f_\phi$, which is the maximal reheating temperature for which our EFT approach remains valid over the entire frequency range. Smaller reheating temperatures $T_\star \ll f_\phi$ result in a suppressed GWB.

The figure reproduces the behaviour expected from the approximations (50) to (52), up to small modifications due to the running of α . For the first two benchmarks $T_\star = m_{\text{Pl}}$ and $T_\star = 10^{15} \text{ GeV}$, one has $f_x > f_{\text{bol}}$. In this case, the spectrum is determined solely by the position of the horizon frequency f_\star , see eq. (50). For $T_\star = m_{\text{Pl}}$, f_\star lies above the range of validity of our approximations, so that Ω_{gw} approximately scales as f^4 . On the other hand, for $T_\star = 10^{15} \text{ GeV}$, $f_\star \approx 3 \cdot 10^7 \text{ Hz}$ lies well within our region of interest. In this case, the GWB scales first as f^4 for $f < f_\star$, and then as f for $f > f_\star$. The third benchmark $T_\star = 10^{10} \text{ GeV}$ is slightly more complex since $f_x < f_{\text{bol}}$, and is captured by eq. (51). Hence, the spectrum exhibits two kinks at $f = f_x \approx 0.1 \text{ Hz}$ and $f = f_{\text{bol}} \approx 9 \cdot 10^4 \text{ Hz}$. Below f_x , the signal grows as f^4 , between f_x and f_{bol} , it grows as $f^{5/2}$, and above f_{bol} , it grows linearly.

Additionally, we observe that only the case $T_\star = 10^{10} \text{ GeV}$ can overcome the equivalent SM background with the same value of T_\star . Indeed, for $T_\star = 10^{15} \text{ GeV}$ and $T_\star = m_{\text{Pl}}$, we always have $T_{\text{entry}} < T_c$ and, hence, GWs are always produced in the Boltzmann regime. For our third benchmark $T_\star = 10^{10} \text{ GeV}$, hydrodynamic contributions dominate the GW production for $f < 0.1 \text{ Hz}$ and the ALP GWB can exceed the SM contribution by ~ 10 orders of magnitude in the LISA frequency band. However, even though it can surpass the SM signal (for the same value of T_{max}) by several orders of magnitude, the ALP contribution remains much too small for any hope of detection at proposed laser interferometer or high frequency GW experiments. We also observe that constraints from N_{eff} are much too weak in that frequency band to constrain hidden sectors. The latter constraints become relevant in the Boltzmann regime [23, 25], where the ALP contribution is subdominant compared to the SM background [34].

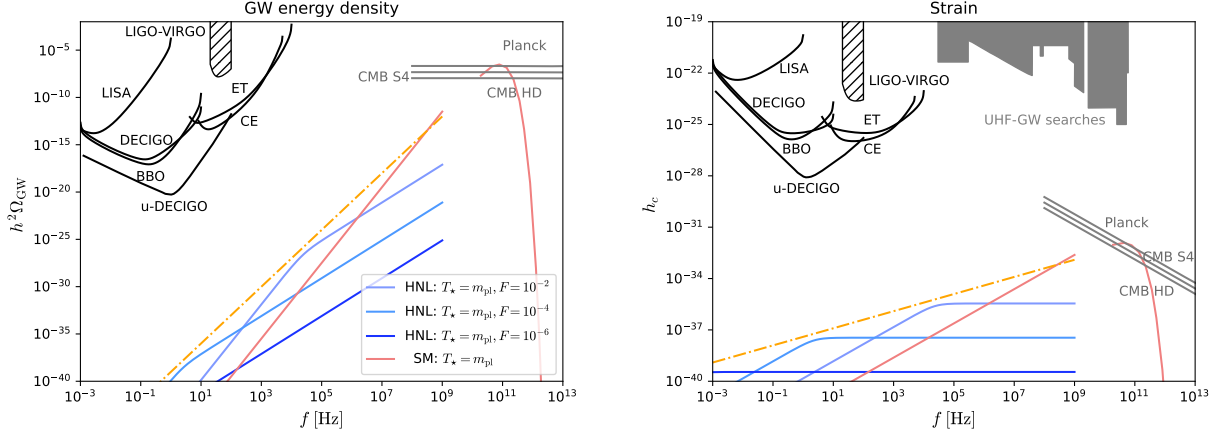


Figure 6: GWB due to thermal fluctuations of a relativistic HNL in the early universe plasma, as measured by the energy density $h^2 \Omega_{\text{GW}}$ (*Left*) and strain h_c (*Right*). For details about the various experimental constraints, see the captions of figures 4 and 5. The light red line shows the expected SM background for $T_{\text{max}} = m_{\text{Pl}}$, see also the caption below figure 4 for more details. The remaining continuous coloured lines show the HNL contribution for various parameter choices. Finally, the dashed orange line corresponds to the upper bound (38)

5.2 Heavy neutral leptons

Heavy neutral leptons (HNL) are a well-motivated extension of the SM that can potentially explain several of its shortcomings [97, 98], including cosmological puzzles, such as the origin of the observed matter-antimatter asymmetry [99] through leptogenesis [100–102] or the dark matter puzzle [103, 104], cf. [105, 106] and [107, 108] for summary articles. An HNL with mass well below the GUT scale may interact only very feebly with the SM.

Its contribution to the cosmological GWB was estimated within the νMSM [102] in [25] but, similarly to the axion case, the impact of the Hubble horizon and the enhancement of its signal due its feeble interactions strength were not accounted for. In the minimal type-I seesaw model, the only relevant interaction is

$$\mathcal{L} \supset F\psi(\tilde{\phi}^\dagger \ell) + \text{h.c.} , \quad (56)$$

where F is the HNL Yukawa coupling, ϕ the SM Higgs doublet, and ℓ a left-handed SM fermion doublet. The optical theorem connects the HNL width Υ_p to its production rate in the early universe plasma, which has been studied extensively, see e.g. [109]. One finds that the momentum-averaged width is given as [110]

$$\Upsilon_{\text{av}} = \gamma(z) \frac{F^2 T}{16\pi} , \quad (57)$$

where γ is a dimensionless function of $z \equiv m/T$. The precise determination of γ is an involved computation, but for our purposes it is sufficient to use the simple approximation

$$\gamma \approx \max\left(0.2, z - \frac{3}{2}\right) . \quad (58)$$

Evaluating the width in the high-temperature limit, this yields the critical frequency

$$f_c = 2.4 \cdot 10^8 \text{ Hz} \times F^2. \quad (59)$$

Figure 6 shows the GW spectrum for different Yukawa couplings and an optimistic maximal temperature $T_\star = m_{\text{Pl}}$,¹⁰ comparing it with expected sensitivities of various prospective gravitational wave detectors. The hydrodynamic regime ($f < f_c$), where the HNL GWB exceeds the SM contribution by several orders of magnitude, is clearly distinct from the Boltzmann regime ($f > f_c$). Although we observe a strong enhancement compared to the SM background, which can be exceeded by up to 10 orders of magnitude, the model independent upper bound (38) forces the signal to lie much below any (currently proposed) detector sensitivities.

6 Discussion and conclusion

In this work, we investigated GW production from thermal fluctuations of hidden particles in the early universe. In contrast to more model-dependent GWBs from e.g. strong first order phase transitions, reheating, or cosmic strings, this background does not rely on deviations from standard cosmology and is therefore much harder to avoid.

To estimate the size of the background, we used the closed time-path (Schwinger-Keldysh) formalism to compute the GW production rate due to fluctuations of a feebly interacting fermion, and combined this rate with prior results for (pseudo-)scalar particles in section 3. Given the striking similarity of equations (19) and (20), we expect that, up to an additional spin multiplicity factor, GW production due to fluctuations of a vector particle is captured by an expression analogous to equation (19). We note in passing that the evaluation of the fermionic production rate at zero energy gives the corresponding contribution to the shear viscosity of the early universe plasma, a quantity that is of interest well beyond its application to GW production.

Using these rates, we then derived phenomenological formulae for GWBs due to thermal fluctuations of generic feebly interacting particles and obtained a model-independent upper bound on such backgrounds in section 4. Our formulae incorporate the well-known fact that super-horizon modes of tensor perturbations are static. This effectively delays the onset of GW production until after horizon re-entry, modifying some prior results for the GWB predicted by the SM [22, 23, 25] (cf. equation (45) and the discussion thereafter). We also investigated backgrounds generated by particles whose width is dominated by non-renormalizable interactions. In principle, these backgrounds encode a plethora of information including the mass of the emitting particle, the dimension of the operator dominating its width, the corresponding UV cutoff scale, and the maximal temperature of the hidden sector plasma. Unfortunately, it seems impossible to observe such GWBs from thermal fluctuations at LISA and other laser interferometers, as the strain induced by the upper bound is still several orders of magnitude below the sensitivity of even beyond next generation experiments such as u-DECIGO. The same applies to present efforts of detecting GWs through electromagnetic

¹⁰ While the equilibration temperature in case of thermal production $T_\star \approx 4 \cdot 10^{-3} m_0 F^2$ tends to be much lower than the Planck scale, HNLs can also be produced at much higher temperature from e.g. inflaton decay [111, 112].

conversion [113] (cf. also [114, 115]), but this is still a young and very active field of research, and it is widely believed that the sensitivity can be increased by several orders of magnitude.¹¹

In section 5, we finally computed the thermal backgrounds from ALPs and HNLs and discussed their properties. We found that, in principle, measuring the different features of such backgrounds would give us access to various model parameters, including the mass of the feebly interacting particle, its coupling strength, and the dimension of the operator dominating its width. We also noticed that the resulting GWBs can be enhanced by 5-10 orders of magnitude compared to the SM background for $f \sim \mathcal{O}(1)$ Hz. Despite this enhancement, these signals unfortunately remain orders of magnitude below the best sensitivity from next-generation laser interferometers or high-frequency GW experiments, consistent with the upper bound found in section 4.2.

Given the pessimistic implications of the upper bound, it is instructive to summarise and question the assumptions under which it was derived, and to assess how it may be avoided. As a general comment, we in practice consider each new particle individually, meaning that our bound constrains the GWB contribution per particle. Its derivation relies on the following assumptions:

1. *Standard Cosmic History.* Our results apply for a standard cosmic history. This amounts to two related but not identical assumptions. (i) In (9) and following we assume that SM degrees of freedom dominate the effective number of radiation degrees of freedom. Relaxing this assumption does not restrict the applicability of the method used here. It would simply require tracking the entropy and temperature evolution in both sectors separately.¹² (ii) We assume that no entropy is transferred between the two sectors. If entropy is transferred from the hidden sector to the SM, the GWB is diluted. If entropy is transferred from the SM to the hidden sector, the GWB can be enhanced, but the details depend on the thermal history of the hidden sector. We sketch how the formulae in section 2 are generalised if these assumptions are relaxed in appendix D.
2. *Focus on the hidden-sector-dominated contribution.* We assume that our computation captures the dominant part of the GWB from hidden sectors. This amounts to two separate assumptions, one of which is conceptual and the other technical in nature. (i) We consider one hidden particle at a time. This is based on the observation that the GWB at low frequencies tends to be dominated by the most weakly interacting particle [22, 23, 25]. If there are several feebly coupled particles, the upper bound in section 4.2 applies to each of them individually. (ii) In our computation of the GW production rate due to a given hidden particle, we focused on contributions from diagrams with a topology as in figure 1 (wave-function type diagrams) with resummed propagators in the loop, which are subject to the enhancement discussed in section 2.1. This enhancement is the

¹¹ However, observing even GWBs that saturate our upper bound has only been shown possible assuming that the interference term between signal and background field in a cavity can be measured at the same accuracy as the signal itself [116], and no method or technology to do this is known (cf. [117] for a discussion).

¹² Note that increasing the number of degrees of freedom enhances the GW production rate, but this enhancement is overcompensated by the subsequent dilution. As a result, models with more degrees of freedom (such as Grand Unified Theories, GUTs) tend to produce a weaker signal than the SM unless the contribution from new particles is enhanced by some mechanism, such as the weakness of their interaction in the present work, cf. section 2.1. However, GUTs can produce GWBs in various other ways, cf. [118, 119].

largest for the particle with the weakest coupling, hence one expects this contribution to dominate in hidden sectors. Our computation does not capture vertex-type corrections such as the diagram in figure 2. Since the enhancement is absent in the Boltzmann regime $k \gg \Upsilon_{\text{av}}$, one can expect contributions from vertex-type diagrams to be of the same order of magnitude as the ones considered here. Hence, we expect order one corrections to GW emission in the Boltzmann regime, the precise computation of which in general may require further resummations (cf. e.g. [120]).

3. *Equilibrium between the sectors.* Throughout sections 4 and 5 (and in particular in figures 4-6) we assumed that the hidden sector is in equilibrium with the SM at a temperature T . When this is not the case, one can distinguish two possibilities. If the hidden sector is in a thermodynamic state that can be described by an effective temperature $T_h \neq T$, then all references to the temperature in the distribution functions have to be replaced with the corresponding values for T_h . For example, this can be the case if hidden sector interactions are strong enough to maintain local thermal equilibrium within each sector, but the portal interaction with the SM is too weak to equilibrate the two sectors with each other. When the hidden sector is in a true non-equilibrium state, our computation can still be applied when using (21) instead of (20), practically replacing the equilibrium distribution functions in the propagators with general phase space distribution functions, provided that the loop integral computed in appendix A is dominated by contributions from the dressed single (quasi)particle poles. While this assumption can in principle be violated (e.g. when the phase space distribution functions exhibit strong peaks, collective excitations play a role, or the continuum contribution from branch-cuts dominates), it can be expected to hold for a wide range of non-equilibrium situations. An immediate consequence of this is that one expects an upper bound such as (37) to hold in non-equilibrium situations, provided that the temperature is replaced by an effective parameter that characterises the occupation numbers. Quantitatively this generalised upper bound can be weaker than the result (37) obtained in equilibrium.

A detailed study on the impact of relaxing one or several of these assumption quantitatively goes beyond the scope of this work. We shall nevertheless briefly comment on what one may expect in two phenomenologically important situations.

Thermal freeze-in describes the incomplete equilibration of some particle species due to a weak coupling and can be relevant for both dark matter production [103, 121] and baryogenesis [101, 102, 106]. Freeze-in scenarios can involve a huge deviation from thermal equilibrium. However, since this is an *underabundance*, the GWB from the concerned particle is expected to be suppressed relative to our upper bound. Recall that the upper bound (37) is the result of a trade-off between two effects that apply irrespective of whether the hidden particle is in equilibrium or not: A smaller hidden particle width Υ_p leads to a stronger enhancement of the GWB per mode, but reduces the range of modes that are enhanced. During freeze-in (when the hidden particles are produced thermally) there is a third effect: A lower Υ_p also implies a slower approach to equilibrium, hence lower occupation numbers. If those can be characterised by an effective temperature $T_h < T$, then it is straightforward to quantify the resulting suppression of the GWB by replacing $T \rightarrow T_h$ in (19) and (20); if not, one has to use the equations in appendix A with the full nonequilibrium distribution in (62) and following.

At a qualitative level it is clear that an underabundance will suppress the contribution to the GWB.

An overabundance, on the other hand, can potentially enhance the GWB. An extreme case of this kind can be realised at the end of cosmic inflation. Indeed, the results obtained in a number of recent works studying graviton emission during reheating [58–61] appear to violate the upper bounds formulated in section 4.2. While the overabundance of inflaton occupation numbers implies that the upper bound should be relaxed, these works appear to compute the GW production rate without accounting for (i) the resummation of wave-function type corrections that is necessary in the hydrodynamic regime (cf. appendix A), and (ii) the suppression of GW emission for super-horizon modes that effectively delays the onset of GW production until they re-enter the horizon.¹³ We expect that systematically incorporating these effects would yield a significant suppression of the resulting GWB. However, it should also be added that some of the assumptions mentioned in point 3 can be violated during reheating. In particular, inflaton decays can produce peaked distribution functions. Moreover, the oscillating inflaton condensate generates effective masses for all particles that couple to it, which can not only lead to non-perturbative particle production due to a parametric resonance, but also modify the perturbative production rate in a way that is not captured by the formulae presented here. Finally, at the onset of reheating the density of particles is low, implying a long mean free path and hence a smaller Υ_{av} than we used. Hence, while the GWB produced from reheating may exceed the upper bound presented here, its quantitative computation requires taking full account of all aforementioned effects and remains an open question.

In summary, we found that the thermal GWB emitted by hidden sectors can dominate over the SM contribution by orders of magnitude in the low frequency regime. In spite of this, the upper bound from section 4.2 and its potential non-equilibrium generalisations imply that the background remains orders of magnitude below the sensitivity of any proposed interferometer if the concerned particles are in thermal equilibrium or underabundant. This pessimistic conclusion may be avoided in situations involving overabundances, such as cosmic reheating, but an accurate formalism to quantify this is still lacking. Hence, while the thermal GWB for a given extension of the SM in principle represents an unavoidable floor for GW measurements, this floor is so low that probing hidden sectors with GWB measurements will almost certainly rely on more model-dependent sources in the foreseeable future.

Acknowledgments

The authors thank Anna Tokareva for making us aware that we forgot to implement the suppression on super-Hubble scales in the initial version of our plots and Diego Blas for a discussion on GW detection in resonant cavities. Y.G. acknowledges the support of the French Community of Belgium through the FRIA grant No. 1.E.063.22F.

¹³ This was previously pointed out in [122, 123].

Appendices

A GW production rate from fermions

To compute the fermionic equivalent of rate (19), we start from the Kubo formula (7) and adapt the strategy used in [34, 39]. The relevant contribution to the stress-energy tensor is

$$T_{ij}(x) \supset \frac{c_X}{4} \bar{\psi}_x \mathfrak{i} D_{ij} \psi_x, \quad \mathfrak{i} D_{ij} = \gamma_i \mathfrak{i} \partial_j + \gamma_j \mathfrak{i} \partial_i, \quad (60)$$

where $\psi_x = \psi(x)$ is either a Dirac or Majorana spinor, evaluated at $x = (t, \mathbf{x})$, and the constant c_X is $c_D = 2$ for a Dirac spinor and $c_M = 1$ for a Majorana spinor. In the interest of full generality, we consider a setup in which the fermion is not necessarily in thermal equilibrium, and use the Schwinger-Keldysh (In-In) formalism of non-equilibrium quantum field theory to evaluate the correlator in (4). For reviews of this formalism, see e.g. [105, 124–126]. The central idea is to evaluate the path-integral along a closed time-path (CTP) running from an initial time t_0 to a final time $t_f = +\infty$ and then back to t_0 . If the state of the system at $t = t_0$ is specified, the CTP path integral can then be used to compute path-ordered, out-of-equilibrium correlation functions

$$\langle T_C \{ \mathcal{O}_1^{a_1} \dots \mathcal{O}_n^{a_n} \} \rangle, \quad (61)$$

where T_C is the time-path ordering operator and the $\mathcal{O}_i^a(x_i)$ are local operators that depend only on field operators evaluated at x_i . Each field operator, and with it each composite operator $\mathcal{O}_i^{a_i}$, picks up an index $a = \pm 1$ that specifies whether it is evaluated along forward (“+”) or backward (“−”) section of the time path. Accordingly, there are four kinds of two-point functions (“++”, “--”, “+-”, and “-+”). The “++” and “--” functions correspond to the usual (anti-)time-ordered propagators, but the two Wightman functions

$$(\mathfrak{i} S_{xy}^>)_{\alpha\beta} = \langle T_C \{ \psi_{x\alpha}^- \bar{\psi}_{y\beta}^+ \} \rangle, \quad (\mathfrak{i} S_{xy}^<)_{\alpha\beta} = \langle T_C \{ \psi_{x\alpha}^+ \bar{\psi}_{y\beta}^- \} \rangle \quad (62)$$

are the most relevant for our present computation, since they determine the impact of finite particle and antiparticle number densities. Working with the Fourier-transformed Wightman functions, we use the ansatz

$$\mathfrak{i} S_p^< = -2n(p_0) S_p^A, \quad \mathfrak{i} S_p^> = 2(1 - n(p_0)) S_p^A, \quad S_{-p}^A = [S_p^A]^T, \quad (63)$$

where $p = (p_0, \mathbf{p})$ is the four-momentum and S_p^A is the spectral function of ψ . In thermal equilibrium, the Kubo-Martin-Schwinger relations imply that the ansatz (63) holds exactly, if $n(p_0)$ is identified with the Fermi-Dirac distribution $n_F(p_0) = [\exp \beta p_0 + 1]^{-1}$. Allowing the fermion ψ to be out-of-equilibrium, we replace n_F with a generic distribution function, $n_F \rightarrow n(p_0, \mathbf{p})$. In principle, ψ has two independent helicity states, each associated with its own distribution function $n_h(p_0)$, but we neglect this helicity dependence. This ansatz is related to the so-called Kadanoff-Baym ansatz, cf. e.g. [127, 128] for an explicit discussion. We emphasize that our computation does not depend on the precise shape of the non-equilibrium distribution functions, provided that they are sufficiently smooth and that the assumptions we make about

the spectral function in appendix B hold. As a result, we expect upper bounds akin to those derived in section 4.2 to hold in out-of-equilibrium scenarios, up to an appropriate modification due to the different phase-space distribution.

We focus on the regime $k \lesssim \Upsilon$, where the leading contribution to Π is generated by the diagram depicted in figure 1. One way to generate the diagram is to Wick contract the correlator (4) without introducing any additional vertices. For a Dirac fermion, this yields

$$\left(\frac{4}{c_D}\right)^2 \langle \{T_{ij}(x), T_{kl}(y)\} \rangle = \langle T_C \{ \bar{\psi}_x (i D_{xij} \psi_x^-) \bar{\psi}_y^+ (i D_{ykl} \psi_y^+) + \bar{\psi}_x^+ (i D_{xij} \psi_x^+) \bar{\psi}_y^- (i D_{ykl} \psi_y^-) \} \rangle$$

$$= -\text{tr}[(i D_{xij} i S_{xy}^>)(i D_{ykl} i S_{yx}^<) + (<, > \leftrightarrow >, <)] , \quad (64)$$

and therefore

$$\Pi(k) = -\frac{c_D^2}{8} \int \frac{d^3 \mathbf{p}}{(2\pi)^3} \int \frac{dp_0}{2\pi} \mathbb{L}^{ij;kl} p_i p_k \text{tr}[\gamma_j i S_p^> \gamma_l i S_{p-k}^< + \gamma_j i S_p^< \gamma_l i S_{p-k}^>] , \quad (65)$$

where $k^\mu = (k, \mathbf{k})$. If ψ is a Majorana fermion, one has to replace $c_D \rightarrow c_M = 1$, but the additional contractions result in a further overall prefactor of 2. In either case, using the ansatz (63), one obtains the generic expression

$$\Pi(k) = c_X \int \frac{d^3 \mathbf{p}}{(2\pi)^3} \int \frac{dp_0}{2\pi} \mathbb{L}^{ij;kl} p_i p_k \text{tr}[\gamma_j S_p^{\mathcal{A}} \gamma_l S_{p-k}^{\mathcal{A}}] \cdot D(p_0^+, p_0^-) , \quad p_\mu^s = p_\mu + \frac{s}{2} k_\mu , \quad (66)$$

where (22) encodes the out-of-equilibrium particle number densities,

$$D(p_0, q_0) = (1 - n(p_0))n(q_0) + n(p_0)(1 - n(q_0)).$$

Using a tree-level or more generic zero-width expression for the spectral function, the integral in (66) would vanish exactly for a finite value of k but diverge for $k = 0$. This divergence is physically related to the fact that a free particle formally has an infinite mean free path, and is regulated by the finite width of the spectral function, resulting in the $l_{\text{av}} \propto 1/\Upsilon$ scaling of the shear viscosity. To capture this effect, it is necessary to resum wave-function type corrections to the spectral function. Following the discussion in appendix B, we write the resummed expression as

$$S_p^{\mathcal{A}} = (\not{p} + m) \frac{\Gamma_p}{\Omega_p^2 + \Gamma_p^2} , \quad \Omega_p = p^2 - m^2 , \quad \Gamma_p \equiv \Gamma(p) = \frac{1}{2} \text{tr}[(\not{p} + m) \Sigma_p^{\mathcal{A}}] , \quad (67)$$

where $\Sigma_p^{\mathcal{A}, \mathcal{H}}$ denotes the (anti-)hermitian self-energy of ψ . The symmetry relation in (63) implies that the width parameter Γ_p has to be odd, $\Gamma_{-p} = -\Gamma_p$. The physical width of the new particle is defined as its on-shell limit,

$$2\epsilon \Upsilon_p = \lim_{p_0 \rightarrow \epsilon} \Gamma_p , \quad \Upsilon_{-p} = \Upsilon_p , \quad \epsilon^2 = \mathbf{p}^2 + m^2 . \quad (68)$$

Inserting the ansatz (67) into equation (66), one finds¹⁴

$$\mathbb{L}^{ij;kl} p_i p_k \text{tr}[\gamma_j S_p^{\mathcal{A}} \gamma_l S_{p-k}^{\mathcal{A}}] = \frac{4p_\perp^2 (p_0^+ p_0^- - \mathbf{p}_+ \mathbf{p}_- - m^2 + p_\perp^2) \Gamma_{p^+} \Gamma_{p^-}}{[\Omega_{p^+}^2 + \Gamma_{p^+}^2][\Omega_{p^-}^2 + \Gamma_{p^-}^2]} , \quad p_\perp^2 \equiv \mathbb{L}_{ij} p^i p^j . \quad (69)$$

¹⁴ The gamma matrices and metric tensor are defined such that $\{\gamma_\mu, \gamma_\nu\} = 2\eta_{\mu\nu}$ with $\eta_{00} = +1$ and $\eta_{ij} = -\delta_{ij}$.

To proceed, we use the residue theorem to evaluate the p_0 integral in (66) in the hydrodynamic regime. In general, the integral receives contributions from two classes of poles: (i) poles associated with the product of distribution functions $D = D(p_0^+, p_0^-)$, and (ii) poles associated with the trace of spectral functions (69). The width parameter Γ is also expected to exhibit a branch-cut at the light-cone $p^2 = 0$. However, for sufficiently small frequencies k and width parameter Γ , the integral (65) is dominated by the regime in which both propagators are close to being on-shell, cf. figures 10 and 11 in [129]¹⁵, where $p^2 > 0$.

As it is the finite width of the spectral function that regulates the integral, only the residues associated with the spectral functions give rise to the enhanced $\propto 1/r$ contributions. Since our primary aim is to extract these enhanced contributions, we neglect the poles of the distribution functions as well as the branch cut of Γ_p , using an analytic continuation to extend the $p^2 > 0$ expression into the regime with $p^2 < 0$. We then close the integration contour along the upper half of the complex plane with $\text{Im } p_0 > 0$. The enhanced contributions are generated by the four poles located at

$$p_0 \rightarrow \epsilon_{s,t} = -\frac{sk}{2} + t \left[\mathbf{p}_s^2 + m^2 + \{i\Gamma_{p^s}\}_{p_0 \rightarrow \epsilon_{s,t}} \right]^{\frac{1}{2}}, \quad (70)$$

where $s, t = \pm 1$. The corresponding residues are

$$\text{Res}_{p_0 \rightarrow \epsilon_{s,t}} \left(\frac{\Gamma_{p^+} \Gamma_{p^-}}{[\Omega_{p^+}^2 + \Gamma_{p^+}^2][\Omega_{p^-}^2 + \Gamma_{p^-}^2]} \right) = \lim_{p_0 \rightarrow \epsilon_{s,t}} \frac{\Gamma_{(p^s - sk)}}{2i(2\epsilon_{s,t} + sk - i\Gamma'_{p^s})[(2sk^\mu p_\mu^s - i\Gamma_{p^s})^2 + \Gamma_{(p^s - sk)}^2]}, \quad (71)$$

where $\Gamma'_p \equiv \partial_{p_0} \Gamma_p$ is an even function of p_0 . To evaluate equation (71), we separately expand both the numerator and denominator to leading order in k and Γ_p . Explicitly, this gives

$$\Gamma_{p^s} \approx \Gamma_{(p^s - sk)} \approx \Gamma_p, \quad \epsilon_{s,t} \approx t\epsilon + i\Upsilon_p - sk \frac{(\epsilon - tp_\parallel)}{2\epsilon}, \quad k^\mu p_\mu^s \approx k(t\epsilon - p_\parallel), \quad (72)$$

where $p_\parallel = \mathbf{k} \cdot \mathbf{p} / k$, and subsequently

$$\text{Res}_{p_0 \rightarrow \epsilon_{s,t}} \left(\frac{\Gamma_{p^+} \Gamma_{p^-}}{[\Omega_{p^+}^2 + \Gamma_{p^+}^2][\Omega_{p^-}^2 + \Gamma_{p^-}^2]} \right) \approx \frac{1}{8i} \frac{\Upsilon_p}{[sk(t\epsilon - p_\parallel) - i t \epsilon \Upsilon_p]^2 + \epsilon^2 \Upsilon_p^2}. \quad (73)$$

Hence, summing over the residues and setting $k \rightarrow 0$ and $\epsilon_{s,t} \rightarrow t\epsilon$ in the remainder of the integrand in (66) gives (21).

The result (20) is a valid approximation of the wave-function type diagram in figure 1. This should hold as long as the integral is dominated by the dressed single quasiparticle poles, which can be expected for momenta $k \ll \Upsilon_p$, provided that the phase space distributions do not feature pronounced peaks. We also expect it to work reasonably well for larger momenta $\Upsilon_p < k \ll T$. The neglected contributions are generated by additional poles of the spectral function (e.g. related to collective excitations [131, 132]), the poles of the distribution function $D(p_0^+, p_0^-)$, and the branch cut of the width parameter Γ_p . The residues of the distribution

¹⁵ While figures 10 and 11 in [129] are useful to illustrate the behaviour of the integral, there is an error in the computation of the damping that was corrected in [130].

function generically scale as Υ_p^2 , and are therefore in any case subleading compared to the residues (71). We expect that a similar suppression is present for the branch cut contribution at sufficiently small momenta, but this may no longer be the case for momenta $k \gg \Upsilon_p$. Furthermore, for momenta $k \sim \pi T$, we can no longer use the approximations (72) or set $k \rightarrow 0$ in the non-singular part of the integrand (66). It is then also necessary to account for additional diagrams such as vertex-type corrections. Finally, we note that the equations used here account for the production of single gravitons, and do not cover the production of coherent multi-graviton states. Emission of multiple hard gravitons with momenta $k \sim \pi T$ was studied in [24], while emission of multiple soft gravitons could e.g. be included by studying the evolution of higher n -point functions.

B Finite temperature spectral function

We consider the spectral function of a massive Dirac or Majorana fermion ψ at finite temperature,

$$S_p^{\mathcal{A}} \equiv \frac{1}{2} \int \frac{d^4 p}{(2\pi)^4} e^{ip(x-y)} \langle \psi_x \otimes \bar{\psi}_y + \bar{\psi}_y \otimes \psi_x \rangle , \quad (74)$$

where \otimes denotes the tensor product in Dirac space. In thermal equilibrium, an exact, if formal, expression is

$$S_p^{\mathcal{A}} = \frac{i}{2} (S_p^r - S_p^a) = \frac{i}{2} \left(\frac{1}{\not{p} - m - \Sigma_p^{\mathcal{H}} + i \Sigma_p^{\mathcal{A}}} - \frac{1}{\not{p} - m - \Sigma_p^{\mathcal{H}} - i \Sigma_p^{\mathcal{A}}} \right) , \quad (75)$$

where S_p^r and S_p^a are the retarded and advanced propagators of ψ and $\Sigma_p^{\mathcal{H}}$ and $\Sigma_p^{\mathcal{A}}$ are its (anti-)hermitian self-energies. Working in the plasma rest frame, they can be cast as

$$\Sigma_p^{\mathcal{X}} = \frac{(\sigma_1^{\mathcal{X}} \not{p} + \tilde{\sigma}_1^{\mathcal{X}} \not{\tilde{p}}) \mathbb{1} + (\sigma_5^{\mathcal{X}} \not{p} + \tilde{\sigma}_5^{\mathcal{X}} \not{\tilde{p}}) \gamma_5}{p^2} + \delta_1^{\mathcal{X}} \mathbb{1} + \delta_5^{\mathcal{X}} \gamma_5 , \quad \tilde{p}^\mu = (|\mathbf{p}|, p_0 \mathbf{p}/|\mathbf{p}|) , \quad (76)$$

where $\mathcal{X} \in \{\mathcal{A}, \mathcal{H}\}$. The quantity \tilde{p}^μ is defined such that $\tilde{p}^2 = -p^2$ and $\tilde{p}p = 0$. This ensures that p^μ and \tilde{p}^μ are linearly independent but span the space of four-vectors with spatial part parallel to \mathbf{p} . The scalar coefficients are

$$\sigma_i^{\mathcal{X}} = \frac{1}{4} \text{tr}[\mathbf{P}_i \not{p} \Sigma_p^{\mathcal{X}}] , \quad \tilde{\sigma}_i^{\mathcal{X}} = -\frac{1}{4} \text{tr}[\mathbf{P}_i \not{\tilde{p}} \Sigma_p^{\mathcal{X}}] , \quad \delta_i^{\mathcal{X}} = \frac{1}{4} \text{tr}[\mathbf{P}_i \Sigma_p^{\mathcal{X}}] , \quad \mathbf{P}_5 = \gamma_5 , \quad \mathbf{P}_1 = \mathbb{1} . \quad (77)$$

Using the decomposition (76), we can recast the retarded and advanced propagators as

$$S_p^{a,r} = \left(\not{p} + m - \overline{\Sigma}_p^{\mathcal{H}} \mp i \overline{\Sigma}_p^{\mathcal{A}} \right) \frac{1}{\Omega_p \mp i \Gamma_p} , \quad \overline{\Sigma}_p^{\mathcal{X}} = \Sigma_p^{\mathcal{X}} - 2\delta_1^{\mathcal{X}} \mathbb{1} , \quad (78)$$

where the functions Ω_p and Γ_p are defined as

$$p^2 \Omega_p \equiv (p^2 - \sigma_1^{\mathcal{H}})^2 - \sigma_1^{\mathcal{A}2} - \tilde{\sigma}_1^{\mathcal{H}2} + \tilde{\sigma}_1^{\mathcal{A}2} - \sigma_5^{\mathcal{H}2} + \sigma_5^{\mathcal{A}2} + \tilde{\sigma}_5^{\mathcal{H}2} - \tilde{\sigma}_5^{\mathcal{A}2} - p^2 [(m + \delta_1^{\mathcal{H}})^2 - \delta_1^{\mathcal{A}2} - \delta_5^{\mathcal{H}2} + \delta_5^{\mathcal{A}2}] , \quad (79a)$$

$$p^2 \Gamma_p \equiv 2[(p^2 - \sigma_1^{\mathcal{H}}) \sigma_1^{\mathcal{A}} + \tilde{\sigma}_1^{\mathcal{H}} \tilde{\sigma}_1^{\mathcal{A}} + \sigma_5^{\mathcal{H}} \sigma_5^{\mathcal{A}} - \tilde{\sigma}_5^{\mathcal{H}} \tilde{\sigma}_5^{\mathcal{A}}] + 2p^2 [\delta_1^{\mathcal{A}} (m + \delta_1^{\mathcal{H}}) - \delta_5^{\mathcal{H}} \delta_5^{\mathcal{A}}] . \quad (79b)$$

The spectral function becomes

$$S_p^{\mathcal{A}} = \left(\not{p} + m - \overline{\Sigma}_p^{\mathcal{H}} \right) \Delta_p - \overline{\Sigma}_p^{\mathcal{A}} \Pi_p , \quad (80)$$

where

$$\Delta_p = \frac{\Gamma_p}{\Omega_p^2 + \Gamma_p^2} , \quad \Pi_p = \frac{\Omega_p}{\Omega_p^2 + \Gamma_p^2} . \quad (81)$$

The condition $\Omega_p \stackrel{!}{=} 0$ determines the location of the mass shell, while $4\Gamma_p = \text{tr}[(\not{p} + m)\Sigma_p^{\mathcal{A}}]$ is proportional to the finite temperature width of the particle. In the zero-width approximation, where $\Gamma_p \rightarrow 0$, one finds

$$\Delta_p \rightarrow \pi \delta(\Omega_p) , \quad \Pi_p \rightarrow \text{P} \left(\frac{1}{\Omega_p} \right) , \quad (82)$$

where $\text{P}(\cdot)$ denotes the principal value. In this limit, the term $\propto \Delta_p$ encodes the propagation of single-particle excitations, encompassing both pseudo-particle and hole modes, while the term $\propto \Pi_p$ encodes the impact of scatterings mediated by these modes. In our computation, we can expand $S_p^{\mathcal{A}}$, Ω , and Γ to leading order in the coefficients (77),

$$S_p^{\mathcal{A}} = (\not{p} + m)\Delta_p + \mathcal{O}(\Sigma^2) , \quad \Omega = p^2 - m^2 , \quad \Gamma = 2(\sigma_1^{\mathcal{A}} + m\delta_1^{\mathcal{A}}) + \mathcal{O}(\Sigma^2) . \quad (83)$$

It is worth pointing out that this approximation, neglecting loop corrections to Ω as well as the Dirac structure of the spectral function, is not always valid. In particular, for soft momenta $|\mathbf{p}| \ll T$, one has to at least keep track of the hard-thermal loop contributions to Ω in order to regulate soft IR divergences and to reproduce the correct spectrum of the fermion propagator, including both massive pseudoparticle and hole modes. In our case, the integral (66) is dominated by hard momenta $|\mathbf{p}| \sim \pi T$ that are close to the lightcone, such that $p^2 \ll T^2$. In this regime, the residue associated with the hole-modes is exponentially suppressed, and they can be neglected as a result, but the pseudoparticle modes still obtain a thermal mass $\propto gT$ that regulates IR divergences and can therefore result in certain logarithmically enhanced contributions. This can be accounted for by promoting m to a temperature dependent thermal mass, $m \rightarrow m(T)$, but it does not impact the validity of our computation. In addition, since there are no more IR divergences to regulate, keeping track of the thermal mass barely modifies our final result (20).

C Supplementary formulae for backgrounds from non-renormalizable interactions

To estimate the final GWB (17) from hidden particles with a width dominated by non-renormalizable interactions, we decompose the high-temperature production rate (26) into a hydrodynamic ($T > T_c$) and Boltzmann ($T < T_c$) contribution,

$$\Pi(k) \stackrel{m \ll T}{\simeq} g_X \frac{16\pi^2}{225} T^5 \begin{cases} 1/2\Upsilon_{\text{av}} & T > T_c \\ 5\Upsilon_{\text{av}}/k^2 & T < T_c \end{cases} . \quad (84)$$

We extract the high-temperature background from the integral in (17) by replacing T_{\min} with m . Using expression (40) for the width Υ_{av} and assuming $d > 4$, one obtains the hydrodynamic contribution

$$h^2 \Omega_{\text{gw}}^{T>m}(f) \stackrel{\text{Hydro}}{\simeq} g_d^- \left(\frac{f}{\text{Hz}} \right)^2 \left[\min \left(\frac{f m}{f_{\text{hyd}} m_{\text{Pl}}}, \frac{T_c}{m_{\text{Pl}}} \right) - \min \left(\frac{f T_{\text{max}}}{f_{\text{max}} m_{\text{Pl}}}, \frac{T_c}{m_{\text{Pl}}} \right) \right] \quad (85)$$

and the Boltzmann contribution

$$h^2 \Omega_{\text{gw}}^{T>m}(f) \stackrel{\text{Boltz.}}{\simeq} g_d^+ \left(\frac{f}{\text{Hz}} \right)^2 \left[\min \left(\frac{f_{\text{max}} T_{\text{max}}}{f m_{\text{Pl}}}, \frac{T_c}{m_{\text{Pl}}} \right) - \min \left(\frac{f_{\text{hyd}} m}{f m_{\text{Pl}}}, \frac{T_c}{m_{\text{Pl}}} \right) \right], \quad (86)$$

where

$$g_d^\pm = \frac{5.3 g_X \cdot 10^{-29}}{2(d-4) \pm 1}, \quad T_{\text{max}} = \max(m, \min(T_{\text{entry}}, T_\star)), \quad f_{\text{max}} = f_c \left(\frac{T_{\text{max}}}{\Lambda} \right)^{2(d-4)}. \quad (87)$$

Adding these two contributions, one obtains the full background

$$h^2 \Omega_{\text{gw}}^{T>m}(f) \simeq g_d^+ \left(\frac{f}{\text{Hz}} \right)^2 \begin{cases} \frac{g_d^-}{g_d^+} \left(\frac{f m}{f_{\text{hyd}} m_{\text{Pl}}} - \frac{f T_{\text{max}}}{f_{\text{max}} m_{\text{Pl}}} \right) & f_{\text{hyd}} > f \\ \left(\frac{T_c}{m_{\text{Pl}}} - \frac{f_{\text{hyd}} m}{f m_{\text{Pl}}} \right) + \frac{g_d^-}{g_d^+} \left(\frac{T_c}{m_{\text{Pl}}} - \frac{f T_{\text{max}}}{f_{\text{max}} m_{\text{Pl}}} \right) & f_{\text{hyd}} < f < f_{\text{max}} \\ \left(\frac{f_{\text{max}} T_{\text{max}}}{f m_{\text{Pl}}} - \frac{f_{\text{hyd}} m}{f m_{\text{Pl}}} \right) & f_{\text{max}} < f \end{cases}. \quad (88)$$

Keeping only the leading terms for each case, one has

$$h^2 \Omega_{\text{gw}}^{T>m}(f) \simeq g_d^+ \left(\frac{f}{\text{Hz}} \right)^2 \begin{cases} \frac{g_d^-}{g_d^+} \frac{f m}{f_{\text{hyd}} m_{\text{Pl}}} & f_{\text{hyd}} > f \\ \left(1 + \frac{g_d^-}{g_d^+} \right) \frac{T_c}{m_{\text{Pl}}} & f_{\text{hyd}} < f < f_{\text{max}} \\ \frac{f_{\text{max}} T_{\text{max}}}{f m_{\text{Pl}}} & f_{\text{max}} < f \end{cases}. \quad (89)$$

In the following, we focus on the case $m < T_\star < \Lambda$. From the definitions (32), (33), and (47) to (49), it then follows that $0 < f_\star - f_{\text{nr}} < f_{\text{bol}} - f_{\text{hyd}}$. From (87), we also find

$$f_{\text{max}} = \begin{cases} f_{\text{hyd}} & f < f_{\text{nr}} \\ f_{\text{int}} & f_{\text{nr}} < f < f_\star \\ f_{\text{bol}} & f_\star < f \end{cases}, \quad f_{\text{int}} \equiv f_x \left(\frac{f}{f_x} \right)^{2(d-4)}, \quad (90)$$

where f_x is defined in (49), and

$$f_{\text{hyd}} < f_{\text{max}} < f_{\text{bol}}, \quad f_{\text{hyd}} = f_x \left(\frac{f_{\text{nr}}}{f_x} \right)^{2(d-4)}, \quad f_{\text{bol}} = f_x \left(\frac{f_\star}{f_x} \right)^{2(d-4)}. \quad (91)$$

For $f < f_{\text{nr}}$, the temperature at horizon entry is below the mass of the hidden particle, so that there is no high-temperature ($T > m$) contribution to the background. Focusing on frequencies $f > f_{\text{nr}}$, we now distinguish four cases:

- Case 1: $f_{\text{nr}} < f_{\text{hyd}} < f_{\star} < f_{\text{bol}}$, which gives

$$h^2 \Omega_{\text{gw}}^{T>m}(f) \simeq g_d^+ \left(\frac{f}{\text{Hz}} \right)^2 \begin{cases} \frac{g_d^-}{g_d^+} \left(\frac{f m}{f_{\text{hyd}} m_{\text{Pl}}} - \frac{f T_{\text{entry}}}{f_{\text{int}} m_{\text{Pl}}} \right) & f_{\text{nr}} < f < f_{\text{hyd}} \\ \left(\frac{T_c}{m_{\text{Pl}}} - \frac{f_{\text{hyd}} m}{f m_{\text{Pl}}} \right) + \frac{g_d^-}{g_d^+} \left(\frac{T_c}{m_{\text{Pl}}} - \frac{f T_{\text{entry}}}{f_{\text{int}} m_{\text{Pl}}} \right) & f_{\text{hyd}} < f < f_{\star} \\ \left(\frac{T_c}{m_{\text{Pl}}} - \frac{f_{\text{hyd}} m}{f m_{\text{Pl}}} \right) + \frac{g_d^-}{g_d^+} \left(\frac{T_c}{m_{\text{Pl}}} - \frac{f T_{\star}}{f_{\text{bol}} m_{\text{Pl}}} \right) & f_{\star} < f < f_{\text{bol}} \\ \left(\frac{f_{\text{bol}} T_{\star}}{f m_{\text{Pl}}} - \frac{f_{\text{hyd}} m}{f m_{\text{Pl}}} \right) & f_{\text{bol}} < f \end{cases} . \quad (92)$$

Keeping only the leading terms, one has

$$h^2 \Omega_{\text{gw}}^{T>m}(f) \simeq g_d^+ \left(\frac{f}{\text{Hz}} \right)^2 \begin{cases} \frac{g_d^-}{g_d^+} \frac{f m}{f_{\text{hyd}} m_{\text{Pl}}} & f_{\text{nr}} < f < f_{\text{hyd}} \\ \left(1 + \frac{g_d^-}{g_d^+} \right) \frac{T_c}{m_{\text{Pl}}} & f_{\text{hyd}} < f < f_{\text{bol}} \\ \frac{f_{\text{bol}} T_{\star}}{f m_{\text{Pl}}} & f_{\text{bol}} < f \end{cases} . \quad (93)$$

- Case 2: $f_{\text{nr}} < f_{\star} < f_{\text{hyd}} < f_{\text{bol}}$, which gives

$$h^2 \Omega_{\text{gw}}^{T>m}(f) \simeq g_d^+ \left(\frac{f}{\text{Hz}} \right)^2 \begin{cases} \frac{g_d^-}{g_d^+} \left(\frac{f m}{f_{\text{hyd}} m_{\text{Pl}}} - \frac{f T_{\text{entry}}}{f_{\text{int}} m_{\text{Pl}}} \right) & f_{\text{nr}} < f < f_{\star} \\ \frac{g_d^-}{g_d^+} \left(\frac{f m}{f_{\text{hyd}} m_{\text{Pl}}} - \frac{f T_{\star}}{f_{\text{bol}} m_{\text{Pl}}} \right) & f_{\star} < f < f_{\text{hyd}} \\ \left(\frac{T_c}{m_{\text{Pl}}} - \frac{f_{\text{hyd}} m}{f m_{\text{Pl}}} \right) + \frac{g_d^-}{g_d^+} \left(\frac{T_c}{m_{\text{Pl}}} - \frac{f T_{\star}}{f_{\text{bol}} m_{\text{Pl}}} \right) & f_{\text{hyd}} < f < f_{\text{bol}} \\ \left(\frac{f_{\text{bol}} T_{\star}}{f m_{\text{Pl}}} - \frac{f_{\text{hyd}} m}{f m_{\text{Pl}}} \right) & f_{\text{bol}} < f \end{cases} . \quad (94)$$

Keeping only the leading terms, one has

$$h^2 \Omega_{\text{gw}}^{T>m}(f) \simeq g_d^+ \left(\frac{f}{\text{Hz}} \right)^2 \begin{cases} \frac{g_d^-}{g_d^+} \frac{f m}{f_{\text{hyd}} m_{\text{Pl}}} & f_{\text{nr}} < f < f_{\text{hyd}} \\ \left(1 + \frac{g_d^-}{g_d^+} \right) \frac{T_c}{m_{\text{Pl}}} & f_{\text{hyd}} < f < f_{\text{bol}} \\ \frac{f_{\text{bol}} T_{\star}}{f m_{\text{Pl}}} & f_{\text{bol}} < f \end{cases} . \quad (95)$$

Notice that this expression is the same as equation (93).

- Case 3: $f_{\text{hyd}} < f_{\text{nr}} < f_{\star} < f_{\text{bol}}$, which gives

$$h^2 \Omega_{\text{gw}}^{T>m}(f) \simeq g_d^+ \left(\frac{f}{\text{Hz}} \right)^2 \begin{cases} \left(\frac{f_{\text{int}} T_{\text{entry}}}{f m_{\text{Pl}}} - \frac{f_{\text{hyd}} m}{f m_{\text{Pl}}} \right) & f_{\text{nr}} < f < f_x \\ \left(\frac{T_c}{m_{\text{Pl}}} - \frac{f_{\text{hyd}} m}{f m_{\text{Pl}}} \right) + \frac{g_d^-}{g_d^+} \left(\frac{T_c}{m_{\text{Pl}}} - \frac{f T_{\text{entry}}}{f_{\text{int}} m_{\text{Pl}}} \right) & f_x < f < f_{\star} \\ \left(\frac{T_c}{m_{\text{Pl}}} - \frac{f_{\text{hyd}} m}{f m_{\text{Pl}}} \right) + \frac{g_d^-}{g_d^+} \left(\frac{T_c}{m_{\text{Pl}}} - \frac{f T_{\star}}{f_{\text{bol}} m_{\text{Pl}}} \right) & f_{\star} < f < f_{\text{bol}} \\ \left(\frac{f_{\text{bol}} T_{\star}}{f m_{\text{Pl}}} - \frac{f_{\text{hyd}} m}{f m_{\text{Pl}}} \right) & f_{\text{bol}} < f \end{cases} . \quad (96)$$

Keeping only the leading terms, one has

$$h^2 \Omega_{\text{gw}}^{T>m}(f) \simeq g_d^+ \left(\frac{f}{\text{Hz}} \right)^2 \begin{cases} \frac{f_{\text{int}} T_{\text{entry}}}{f m_{\text{Pl}}} & f_{\text{nr}} < f < f_x \\ \left(1 + \frac{g_d^-}{g_d^+} \right) \frac{T_c}{m_{\text{Pl}}} & f_x < f < f_{\text{bol}} \\ \frac{f_{\text{bol}} T_{\star}}{f m_{\text{Pl}}} & f_{\text{bol}} < f \end{cases} . \quad (97)$$

- Case 4: $f_{\text{hyd}} < f_{\text{nr}}, f_{\text{bol}} < f_{\star}$, which gives

$$h^2 \Omega_{\text{gw}}^{T>m}(f) \simeq g_d^+ \left(\frac{f}{\text{Hz}} \right)^2 \begin{cases} \left(\frac{f_{\text{int}} T_{\text{entry}}}{f m_{\text{Pl}}} - \frac{f_{\text{hyd}} m}{f m_{\text{Pl}}} \right) & f_{\text{nr}} < f < f_{\star} \\ \left(\frac{f_{\text{bol}} T_{\star}}{f m_{\text{Pl}}} - \frac{f_{\text{hyd}} m}{f m_{\text{Pl}}} \right) & f_{\star} < f \end{cases}. \quad (98)$$

Keeping only the leading terms, one has

$$h^2 \Omega_{\text{gw}}^{T>m}(f) \simeq g_d^+ \left(\frac{f}{\text{Hz}} \right)^2 \begin{cases} \frac{f_{\text{int}} T_{\text{entry}}}{f m_{\text{Pl}}} & f_{\text{nr}} < f < f_{\star} \\ \frac{f_{\text{bol}} T_{\star}}{f m_{\text{Pl}}} & f_{\star} < f \end{cases}. \quad (99)$$

Considering the limit of a light hidden particle, where $f_{\text{hyd}}, f_{\text{nr}} \rightarrow 0$, only two cases survive:

- Case 3, which gives

$$h^2 \Omega_{\text{gw}}^{T>m}(f) \simeq g_d^+ \left(\frac{f}{\text{Hz}} \right)^2 \begin{cases} \frac{f_{\text{int}} T_{\text{entry}}}{f m_{\text{Pl}}} & f < f_x \\ \frac{T_c}{m_{\text{Pl}}} + \frac{g_d^-}{g_d^+} \left(\frac{T_c}{m_{\text{Pl}}} - \frac{f T_{\text{entry}}}{f_{\text{int}} m_{\text{Pl}}} \right) & f_x < f < f_{\star} \\ \frac{T_c}{m_{\text{Pl}}} + \frac{g_d^-}{g_d^+} \left(\frac{T_c}{m_{\text{Pl}}} - \frac{f T_{\star}}{f_{\text{bol}} m_{\text{Pl}}} \right) & f_{\star} < f < f_{\text{bol}} \\ \frac{f_{\text{bol}} T_{\star}}{f m_{\text{Pl}}} & f_{\text{bol}} < f \end{cases}. \quad (100)$$

- Case 4, which gives

$$h^2 \Omega_{\text{gw}}^{T>m}(f) \simeq g_d^+ \left(\frac{f}{\text{Hz}} \right)^2 \begin{cases} \frac{f_{\text{int}} T_{\text{entry}}}{f m_{\text{Pl}}} & f < f_{\star} \\ \frac{f_{\text{bol}} T_{\star}}{f m_{\text{Pl}}} & f_{\star} < f \end{cases}. \quad (101)$$

D More general cosmic histories

Integrating the graviton equation of motion (3), and using the numerical constants in (13), one has

$$h^2 \Omega_{\text{gw}}(f) \approx 1.31 \cdot 10^{-37} \times \left(\frac{f}{\text{Hz}} \right)^3 \int_{t_i}^{t_f} dt \frac{a}{a_0 T_0} \frac{\Pi(2\pi f a_0/a)}{m_{\text{Pl}}^2}, \quad (102)$$

where t_i is the initial time at the onset and t_f the final time at the end of GW production. In order to evaluate the integral, one has to supply expressions for a and Π as functions of time. In section 2.2, we assumed that the SM is in kinetic equilibrium, that it dominates the overall energy budget of the universe, and that there is no entropy exchange with other sectors. If the SM does not dominate the energy budget but the other two assumptions do remain valid, one obtains

$$h^2 \Omega_{\text{gw}}(f) \approx 2.02 \cdot 10^{-38} \times \left(\frac{f}{\text{Hz}} \right)^3 \times \int_{T_{\text{min}}}^{T_{\text{max}}} \frac{dT'}{m_{\text{Pl}}} \frac{\Pi(2\pi f a_0/a')}{8T'^4} \left(\frac{\rho_{\text{SM}}}{\rho_{\text{tot}}} \right)^{\frac{1}{2}}, \quad (103)$$

generalizing equation (15). This expression is strictly smaller than equation (15), so that it does not affect the upper bounds derived in section 4.2. Of course, this does not imply that the GWB is always smaller than in cases where the SM dominates the energy budget, since the impact of new particles may also enhance the production rate $\Pi(2\pi f a_0/a')$, while still respecting the upper bounds in section 4.2.

If significant amounts of entropy are transferred between the SM and other sectors, it becomes necessary to solve the Friedmann equations in order to directly obtain the time-evolution of the SM temperature T and the Hubble rate H . If T and H are known monotonous functions of the scale-factor, one can rewrite equation (102) as

$$h^2 \Omega_{\text{gw}}(f) \approx 2.02 \cdot 10^{-38} \times \left(\frac{f}{\text{Hz}}\right)^3 \int_{T_{\min}}^{T_{\max}} \frac{dT'}{m_{\text{Pl}}} \frac{\Pi(2\pi f a_0/a)}{8T'^4} \left| \frac{d \ln a}{d \ln T'} \right| \left(\frac{T'}{\bar{T}}\right) \left(\frac{\rho_{\text{SM}}}{\rho_{\text{tot}}}\right)^{\frac{1}{2}}, \quad (104)$$

where

$$\bar{T} \equiv \frac{a_0 T_0}{a} \left[\frac{g_s^{\text{SM}}(T_0)}{g_s^{\text{SM}}(\bar{T})} \right]^{1/3} \quad (105)$$

is what the SM temperature would be in the absence of entropy transfers. Using the SM production rate (16), one obtains the final background from SM physics

$$h^2 \Omega_{\text{gw}}^{\text{SM}}(f) \approx 1.03 \cdot 10^{-36} \times \left(\frac{f}{\text{Hz}}\right)^3 \int_{T_{\min}}^{T_{\max}} \frac{dT'}{m_{\text{Pl}}} \left| \frac{d \ln a}{d \ln T'} \right| \left(\frac{T'}{\bar{T}}\right) \left(\frac{\rho_{\text{SM}}}{\rho_{\text{tot}}}\right)^{\frac{1}{2}}, \quad (106)$$

which extends (17) to more general cosmic histories. Note that the product $\left| \frac{d \ln a}{d \ln T'} \right| \frac{T'}{\bar{T}}$ in (104) also makes it possible to describe GWB production without entropy transfer between sectors during periods with an expansion history that deviated from radiation domination, which can e.g. be realised during reheating.

References

- [1] *LISA*. ‘Laser Interferometer Space Antenna’ (Feb. 2017). arXiv: 1702.00786 [astro-ph.IM].
- [2] C. Caprini et al. ‘Science with the space-based interferometer eLISA. II: Gravitational waves from cosmological phase transitions’. In: *JCAP* 04 (2016), p. 001. DOI: 10.1088/1475-7516/2016/04/001. arXiv: 1512.06239 [astro-ph.CO]. №: DESY-15-246.
- [3] D. J. Weir. ‘Gravitational waves from a first order electroweak phase transition: a brief review’. In: *Phil. Trans. Roy. Soc. Lond. A* 376.2114 (2018), p. 20170126. DOI: 10.1098/rsta.2017.0126. arXiv: 1705.01783 [hep-ph]. №: HIP-2017-06-TH.
- [4] C. Caprini et al. ‘Detecting gravitational waves from cosmological phase transitions with LISA: an update’. In: *JCAP* 03 (2020), p. 024. DOI: 10.1088/1475-7516/2020/03/024. arXiv: 1910.13125 [astro-ph.CO]. №: DESY-19-159, IPPP/19/27, HIP-2019-14/TH, MITP/19-066, and IFT-UAM/CSIC-19-139.

- [5] *LISA Cosmology Working Group*. ‘Cosmology with the Laser Interferometer Space Antenna’. In: *Living Rev. Rel.* 26.1 (2023), p. 5. DOI: 10.1007/s41114-023-00045-2. arXiv: 2204.05434 [astro-ph.CO]. №: LISA CosWG-22-03 and FERMILAB-PUB-22-349-SCD.
- [6] M. Punturo et al. ‘The Einstein Telescope: A third-generation gravitational wave observatory’. In: *Class. Quant. Grav.* 27 (2010). Ed. by F. Ricci, p. 194002. DOI: 10.1088/0264-9381/27/19/194002.
- [7] M. Maggiore et al. ‘Science Case for the Einstein Telescope’. In: *JCAP* 03 (2020), p. 050. DOI: 10.1088/1475-7516/2020/03/050. arXiv: 1912.02622 [astro-ph.CO].
- [8] S. Kawamura et al. ‘The Japanese space gravitational wave antenna: DECIGO’. In: *Class. Quant. Grav.* 28 (2011). Ed. by S. Buchman and K.-X. Sun, p. 094011. DOI: 10.1088/0264-9381/28/9/094011.
- [9] S. Sato et al. ‘The status of DECIGO’. In: *J. Phys. Conf. Ser.* 840.1 (2017). Ed. by D. Giardini and P. Jetzer, p. 012010. DOI: 10.1088/1742-6596/840/1/012010.
- [10] N. Seto, S. Kawamura, and T. Nakamura. ‘Possibility of direct measurement of the acceleration of the universe using 0.1-Hz band laser interferometer gravitational wave antenna in space’. In: *Phys. Rev. Lett.* 87 (2001), p. 221103. DOI: 10.1103/PhysRevLett.87.221103. arXiv: astro-ph/0108011.
- [11] H. Kudoh, A. Taruya, T. Hiramatsu, and Y. Himemoto. ‘Detecting a gravitational-wave background with next-generation space interferometers’. In: *Phys. Rev. D* 73 (2006), p. 064006. DOI: 10.1103/PhysRevD.73.064006. arXiv: gr-qc/0511145. №: UTAP-544 and RESCEU-37-05.
- [12] J. Crowder and N. J. Cornish. ‘Beyond LISA: Exploring future gravitational wave missions’. In: *Phys. Rev. D* 72 (2005), p. 083005. DOI: 10.1103/PhysRevD.72.083005. arXiv: gr-qc/0506015.
- [13] G. M. Harry, P. Fritschel, D. A. Shaddock, W. Folkner, and E. S. Phinney. ‘Laser interferometry for the big bang observer’. In: *Class. Quant. Grav.* 23 (2006). [Erratum: *Class. Quant. Grav.* 23, 7361 (2006)], pp. 4887–4894. DOI: 10.1088/0264-9381/23/15/008.
- [14] V. Corbin and N. J. Cornish. ‘Detecting the cosmic gravitational wave background with the big bang observer’. In: *Class. Quant. Grav.* 23 (2006), pp. 2435–2446. DOI: 10.1088/0264-9381/23/7/014. arXiv: gr-qc/0512039.
- [15] N. Aggarwal et al. ‘Challenges and opportunities of gravitational-wave searches at MHz to GHz frequencies’. In: *Living Rev. Rel.* 24.1 (2021), p. 4. DOI: 10.1007/s41114-021-00032-5. arXiv: 2011.12414 [gr-qc]. №: CERN-TH-2020-185, HIP-2020-28/TH, DESY 20-195, CERN-TH-2020-185, HIP-2020-28/TH, and DESY 20-195.
- [16] M. Kamionkowski, A. Kosowsky, and M. S. Turner. ‘Gravitational radiation from first order phase transitions’. In: *Phys. Rev. D* 49 (1994), pp. 2837–2851. DOI: 10.1103/PhysRevD.49.2837. arXiv: astro-ph/9310044. №: IASSNS-HEP-93-44 and FERMILAB-PUB-93-235-A.

- [17] R. Apreda, M. Maggiore, A. Nicolis, and A. Riotto. ‘Gravitational waves from electroweak phase transitions’. In: *Nucl. Phys. B* 631 (2002), pp. 342–368. DOI: 10.1016/S0550-3213(02)00264-X. arXiv: gr-qc/0107033. №: UGVA-DPT-07-1096.
- [18] C. Grojean and G. Servant. ‘Gravitational Waves from Phase Transitions at the Electroweak Scale and Beyond’. In: *Phys. Rev. D* 75 (2007), p. 043507. DOI: 10.1103/PhysRevD.75.043507. arXiv: hep-ph/0607107. №: CERN-PH-TH-2006-125.
- [19] C. Caprini and D. G. Figueroa. ‘Cosmological Backgrounds of Gravitational Waves’. In: *Class. Quant. Grav.* 35.16 (2018), p. 163001. DOI: 10.1088/1361-6382/aac608. arXiv: 1801.04268 [astro-ph.CO].
- [20] M. Giovannini. ‘Primordial backgrounds of relic gravitons’. In: *Prog. Part. Nucl. Phys.* 112 (2020), p. 103774. DOI: 10.1016/j.pnpnp.2020.103774. arXiv: 1912.07065 [astro-ph.CO]. №: CERN-TH-2019-166.
- [21] A. Dasgupta, P. S. B. Dev, A. Ghoshal, and A. Mazumdar. ‘Gravitational wave pathway to testable leptogenesis’. In: *Phys. Rev. D* 106.7 (2022), p. 075027. DOI: 10.1103/PhysRevD.106.075027. arXiv: 2206.07032 [hep-ph].
- [22] J. Ghiglieri and M. Laine. ‘Gravitational wave background from Standard Model physics: Qualitative features’. In: *JCAP* 07 (2015), p. 022. DOI: 10.1088/1475-7516/2015/07/022. arXiv: 1504.02569 [hep-ph].
- [23] J. Ghiglieri, G. Jackson, M. Laine, and Y. Zhu. ‘Gravitational wave background from Standard Model physics: Complete leading order’. In: *JHEP* 07 (2020), p. 092. DOI: 10.1007/JHEP07(2020)092. arXiv: 2004.11392 [hep-ph].
- [24] J. Ghiglieri, J. Schütte-Engel, and E. Speranza. ‘Freezing-In Gravitational Waves’ (Nov. 2022). arXiv: 2211.16513 [hep-ph].
- [25] A. Ringwald, J. Schütte-Engel, and C. Tamarit. ‘Gravitational Waves as a Big Bang Thermometer’. In: *JCAP* 03 (2021), p. 054. DOI: 10.1088/1475-7516/2021/03/054. arXiv: 2011.04731 [hep-ph]. №: DESY 20-187, DESY-20-187, and TUM-HEP-1293-20.
- [26] A. Hosoya, M.-a. Sakagami, and M. Takao. ‘Nonequilibrium Thermodynamics in Field Theory: Transport Coefficients’. In: *Annals Phys.* 154 (1984), p. 229. DOI: 10.1016/0003-4916(84)90144-1. №: OU-HET-53.
- [27] S. Jeon. ‘Hydrodynamic transport coefficients in relativistic scalar field theory’. In: *Phys. Rev. D* 52 (1995), pp. 3591–3642. DOI: 10.1103/PhysRevD.52.3591. arXiv: hep-ph/9409250. №: UW-PT-94-09.
- [28] S. Jeon and L. G. Yaffe. ‘From quantum field theory to hydrodynamics: Transport coefficients and effective kinetic theory’. In: *Phys. Rev. D* 53 (1996), pp. 5799–5809. DOI: 10.1103/PhysRevD.53.5799. arXiv: hep-ph/9512263. №: UW-PT-95-09.
- [29] P. Agrawal et al. ‘Feebly-interacting particles: FIPs 2020 workshop report’. In: *Eur. Phys. J. C* 81.11 (2021), p. 1015. DOI: 10.1140/epjc/s10052-021-09703-7. arXiv: 2102.12143 [hep-ph].

- [30] S. Alekhin et al. ‘A facility to Search for Hidden Particles at the CERN SPS: the SHiP physics case’. In: *Rept. Prog. Phys.* 79.12 (2016), p. 124201. DOI: 10.1088/0034-4885/79/12/124201. arXiv: 1504.04855 [hep-ph]. №: CERN-SPSC-2015-017 and SPSC-P-350-ADD-1.
- [31] D. Curtin et al. ‘Long-Lived Particles at the Energy Frontier: The MATHUSLA Physics Case’. In: *Rept. Prog. Phys.* 82.11 (2019), p. 116201. DOI: 10.1088/1361-6633/ab28d6. arXiv: 1806.07396 [hep-ph]. №: FERMILAB-PUB-18-264-T.
- [32] C. Arina, J. Hajer, and P. Klose. ‘Portal Effective Theories. A framework for the model independent description of light hidden sector interactions’. In: *JHEP* 09 (2021), p. 063. DOI: 10.1007/JHEP09(2021)063. arXiv: 2105.06477 [hep-ph].
- [33] R. Jinno, B. Shakya, and J. van de Vis. ‘Gravitational Waves from Feebly Interacting Particles in a First Order Phase Transition’ (Nov. 2022). arXiv: 2211.06405 [gr-qc]. №: DESY-22-172, IFT-UAM/CSIC-22-140, MITP-22-095, and RESCEU-22/22.
- [34] P. Klose, M. Laine, and S. Procacci. ‘Gravitational wave background from non-Abelian reheating after axion-like inflation’. In: *JCAP* 05 (2022), p. 021. DOI: 10.1088/1475-7516/2022/05/021. arXiv: 2201.02317 [hep-ph].
- [35] P. Klose, M. Laine, and S. Procacci. ‘Gravitational wave background from vacuum and thermal fluctuations during axion-like inflation’. In: *JCAP* 12 (2022), p. 020. DOI: 10.1088/1475-7516/2022/12/020. arXiv: 2210.11710 [hep-ph].
- [36] P. B. Arnold, G. D. Moore, and L. G. Yaffe. ‘Transport coefficients in high temperature gauge theories. 1. Leading log results’. In: *JHEP* 11 (2000), p. 001. DOI: 10.1088/1126-6708/2000/11/001. arXiv: hep-ph/0010177. №: UW-PT-00-15.
- [37] P. B. Arnold, G. D. Moore, and L. G. Yaffe. ‘Effective kinetic theory for high temperature gauge theories’. In: *JHEP* 01 (2003), p. 030. DOI: 10.1088/1126-6708/2003/01/030. arXiv: hep-ph/0209353.
- [38] P. B. Arnold, G. D. Moore, and L. G. Yaffe. ‘Transport coefficients in high temperature gauge theories. 2. Beyond leading log’. In: *JHEP* 05 (2003), p. 051. DOI: 10.1088/1126-6708/2003/05/051. arXiv: hep-ph/0302165.
- [39] G. Jackson and M. Laine. ‘Hydrodynamic fluctuations from a weakly coupled scalar field’. In: *Eur. Phys. J. C* 78.4 (2018), p. 304. DOI: 10.1140/epjc/s10052-018-5791-3. arXiv: 1803.01871 [hep-ph].
- [40] M. S. Turner. ‘Coherent Scalar Field Oscillations in an Expanding Universe’. In: *Phys. Rev. D* 28 (1983), p. 1243. DOI: 10.1103/PhysRevD.28.1243. №: EFI-83-29-CHICAGO.
- [41] P. G. Ferreira and M. Joyce. ‘Cosmology with a primordial scaling field’. In: *Phys. Rev. D* 58 (1998), p. 023503. DOI: 10.1103/PhysRevD.58.023503. arXiv: astro-ph/9711102. №: CFPA-97-TH-20.
- [42] R. Catena, N. Fornengo, M. Pato, L. Pieri, and A. Masiero. ‘Thermal Relics in Modified Cosmologies: Bounds on Evolution Histories of the Early Universe and Cosmological Boosts for PAMELA’. In: *Phys. Rev. D* 81 (2010), p. 123522. DOI: 10.1103/PhysRevD.81.123522. arXiv: 0912.4421 [astro-ph.CO]. №: DFTT-71-2009.

- [43] D. J. Fixsen. ‘The Temperature of the Cosmic Microwave Background’. In: *Astrophys. J.* 707 (2009), pp. 916–920. DOI: 10.1088/0004-637X/707/2/916. arXiv: 0911.1955 [astro-ph.CO].
- [44] K. Saikawa and S. Shirai. ‘Primordial gravitational waves, precisely: The role of thermodynamics in the Standard Model’. In: *JCAP* 05 (2018), p. 035. DOI: 10.1088/1475-7516/2018/05/035. arXiv: 1803.01038 [hep-ph]. №: IPMU18-0037 and MPP-2018-19.
- [45] *Particle Data Group*. ‘Review of Particle Physics’. In: *PTEP* 2022 (2022), p. 083C01. DOI: 10.1093/ptep/ptac097.
- [46] M. Giovannini. ‘Gravitational waves constraints on postinflationary phases stiffer than radiation’. In: *Phys. Rev. D* 58 (1998), p. 083504. DOI: 10.1103/PhysRevD.58.083504. arXiv: hep-ph/9806329.
- [47] K. Mukaida and M. Yamada. ‘Thermalization Process after Inflation and Effective Potential of Scalar Field’. In: *JCAP* 02 (2016), p. 003. DOI: 10.1088/1475-7516/2016/02/003. arXiv: 1506.07661 [hep-ph]. №: IPMU-15-0096.
- [48] M. Breitbach, J. Kopp, E. Madge, T. Opferkuch, and P. Schwaller. ‘Dark, Cold, and Noisy: Constraining Secluded Hidden Sectors with Gravitational Waves’. In: *JCAP* 07 (2019), p. 007. DOI: 10.1088/1475-7516/2019/07/007. arXiv: 1811.11175 [hep-ph]. №: CERN-TH-2018-255 and MITP/18-115.
- [49] K. Freese and M. W. Winkler. ‘Dark matter and gravitational waves from a dark big bang’. In: *Phys. Rev. D* 107.8 (2023), p. 083522. DOI: 10.1103/PhysRevD.107.083522. arXiv: 2302.11579 [astro-ph.CO]. №: UTWI-06-2023 and NORDITA-2023-003.
- [50] T. Tenkanen and V. Vaskonen. ‘Reheating the Standard Model from a hidden sector’. In: *Phys. Rev. D* 94.8 (2016), p. 083516. DOI: 10.1103/PhysRevD.94.083516. arXiv: 1606.00192 [astro-ph.CO]. №: HIP-2016-18-TH.
- [51] F. Ertas, F. Kahlhoefer, and C. Tasillo. ‘Turn up the volume: listening to phase transitions in hot dark sectors’. In: *JCAP* 02.02 (2022), p. 014. DOI: 10.1088/1475-7516/2022/02/014. arXiv: 2109.06208 [astro-ph.CO]. №: TTK-21-36 and DESY-22-014.
- [52] A. R. Liddle and S. M. Leach. ‘How long before the end of inflation were observable perturbations produced?’ In: *Phys. Rev. D* 68 (2003), p. 103503. DOI: 10.1103/PhysRevD.68.103503. arXiv: astro-ph/0305263.
- [53] J. Martin and C. Ringeval. ‘First CMB Constraints on the Inflationary Reheating Temperature’. In: *Phys. Rev. D* 82 (2010), p. 023511. DOI: 10.1103/PhysRevD.82.023511. arXiv: 1004.5525 [astro-ph.CO].
- [54] P. Adshead, R. Easther, J. Pritchard, and A. Loeb. ‘Inflation and the Scale Dependent Spectral Index: Prospects and Strategies’. In: *JCAP* 02 (2011), p. 021. DOI: 10.1088/1475-7516/2011/02/021. arXiv: 1007.3748 [astro-ph.CO].
- [55] M. Drewes and L. Ming. ‘Connecting Cosmic Inflation to Particle Physics with Lite-BIRD, CMB S4, EUCLID and SKA’. In: *Phys. Rev. Lett.* (2024), in press. arXiv: 2208.07609 [hep-ph].

- [56] M. Drewes, L. Ming, and I. Oldengott. ‘LiteBIRD and CMB-S₄ sensitivities to reheating in plateau models of inflation’. In: *JCAP* 05 (2024), p. 081. DOI: 10.1088/1475-7516/2024/05/081. arXiv: 2303.13503 [hep-ph].
- [57] S. Weinberg. *Cosmology*. 2008. ISBN: 978-0-19-852682-7.
- [58] S. Kanemura and K. Kaneta. ‘Gravitational Waves from Particle Decays during Reheating’ (Oct. 2023). arXiv: 2310.12023 [hep-ph]. №: OU-HET-1206.
- [59] N. Bernal, S. Cléry, Y. Mambrini, and Y. Xu. ‘Probing Reheating with Graviton Bremsstrahlung’ (Nov. 2023). arXiv: 2311.12694 [hep-ph]. №: MITP-23-065.
- [60] B. Barman, N. Bernal, Y. Xu, and Ó. Zapata. ‘Gravitational wave from graviton Bremsstrahlung during reheating’. In: *JCAP* 05 (2023), p. 019. DOI: 10.1088/1475-7516/2023/05/019. arXiv: 2301.11345 [hep-ph].
- [61] B. Barman, N. Bernal, Y. Xu, and Ó. Zapata. ‘Bremsstrahlung-induced gravitational waves in monomial potentials during reheating’. In: *Phys. Rev. D* 108.8 (2023), p. 083524. DOI: 10.1103/PhysRevD.108.083524. arXiv: 2305.16388 [hep-ph].
- [62] E. W. Kolb and M. S. Turner. *The Early Universe*. Vol. 69. 1990. ISBN: 978-0-201-62674-2. DOI: 10.1201/9780429492860. №: FERMILAB-BOOK-1990-01.
- [63] K. Schmitz. ‘New Sensitivity Curves for Gravitational-Wave Signals from Cosmological Phase Transitions’. In: *JHEP* 01 (2021), p. 097. DOI: 10.1007/JHEP01(2021)097. arXiv: 2002.04615 [hep-ph]. №: CERN-TH-2020-018.
- [64] A. Ringwald, K. Saikawa, and C. Tamarit. ‘Primordial gravitational waves in a minimal model of particle physics and cosmology’. In: *JCAP* 02 (2021), p. 046. DOI: 10.1088/1475-7516/2021/02/046. arXiv: 2009.02050 [hep-ph]. №: DESY 20-135, DESY-20-135, KANAZAWA-20-06, and TUM-HEP-1279-20.
- [65] E. Thrane and J. D. Romano. ‘Sensitivity curves for searches for gravitational-wave backgrounds’. In: *Phys. Rev. D* 88.12 (2013), p. 124032. DOI: 10.1103/PhysRevD.88.124032. arXiv: 1310.5300 [astro-ph.IM].
- [66] *KAGRA, Virgo, LIGO Scientific*. ‘Upper limits on the isotropic gravitational-wave background from Advanced LIGO and Advanced Virgo’s third observing run’. In: *Phys. Rev. D* 104.2 (2021), p. 022004. DOI: 10.1103/PhysRevD.104.022004. arXiv: 2101.12130 [gr-qc]. №: LIGO-DCC-P2000314.
- [67] *Planck*. ‘Planck 2018 results. VI. Cosmological parameters’. In: *Astron. Astrophys.* 641 (2020). [Erratum: *Astron. Astrophys.* 652, C4 (2021)], A6. DOI: 10.1051/0004-6361/201833910. arXiv: 1807.06209 [astro-ph.CO].
- [68] *CMB-S₄*. ‘CMB-S₄ Science Book, First Edition’ (Oct. 2016). arXiv: 1610.02743 [astro-ph.CO]. №: FERMILAB-FN-1024-A-AE.
- [69] *CMB-HD*. ‘Snowmass2021 CMB-HD White Paper’ (Mar. 2022). arXiv: 2203.05728 [astro-ph.CO]. №: FERMILAB-PUB-22-344-PPD.
- [70] R. D. Peccei and H. R. Quinn. ‘Constraints Imposed by CP Conservation in the Presence of Instantons’. In: *Phys. Rev. D* 16 (1977), pp. 1791–1797. DOI: 10.1103/PhysRevD.16.1791. №: ITP-572-STANFORD.

- [71] R. D. Peccei and H. R. Quinn. ‘CP Conservation in the Presence of Instantons’. In: *Phys. Rev. Lett.* 38 (1977), pp. 1440–1443. DOI: 10.1103/PhysRevLett.38.1440. №: ITP-568-STANFORD.
- [72] S. Weinberg. ‘A New Light Boson?’ In: *Phys. Rev. Lett.* 40 (1978), pp. 223–226. DOI: 10.1103/PhysRevLett.40.223. №: HUTP-77/A074.
- [73] F. Wilczek. ‘Problem of Strong P and T Invariance in the Presence of Instantons’. In: *Phys. Rev. Lett.* 40 (1978), pp. 279–282. DOI: 10.1103/PhysRevLett.40.279. №: PRINT-77-0939 (COLUMBIA).
- [74] L. Di Luzio, M. Giannotti, E. Nardi, and L. Visinelli. ‘The landscape of QCD axion models’. In: *Phys. Rept.* 870 (2020), pp. 1–117. DOI: 10.1016/j.physrep.2020.06.002. arXiv: 2003.01100 [hep-ph]. №: DESY 20-036 and DESY-20-036.
- [75] W.-Y. Ai, J. S. Cruz, B. Garbrecht, and C. Tamarit. ‘Consequences of the order of the limit of infinite spacetime volume and the sum over topological sectors for CP violation in the strong interactions’. In: *Phys. Lett. B* 822 (2021), p. 136616. DOI: 10.1016/j.physletb.2021.136616. arXiv: 2001.07152 [hep-th]. №: TUM-HEP-1249/20 and CP3-20-02.
- [76] J. Preskill, M. B. Wise, and F. Wilczek. ‘Cosmology of the Invisible Axion’. In: *Phys. Lett. B* 120 (1983). Ed. by M. A. Srednicki, pp. 127–132. DOI: 10.1016/0370-2693(83)90637-8. №: HUTP-82-A048 and NSF-ITP-82-103.
- [77] L. F. Abbott and P. Sikivie. ‘A Cosmological Bound on the Invisible Axion’. In: *Phys. Lett. B* 120 (1983). Ed. by M. A. Srednicki, pp. 133–136. DOI: 10.1016/0370-2693(83)90638-X. №: PRINT-82-0695 (BRANDEIS).
- [78] M. Dine and W. Fischler. ‘The Not So Harmless Axion’. In: *Phys. Lett. B* 120 (1983). Ed. by M. A. Srednicki, pp. 137–141. DOI: 10.1016/0370-2693(83)90639-1. №: UPR-0201T.
- [79] C. B. Adams et al. ‘Axion Dark Matter’. *Snowmass 2021*. Mar. 2022. arXiv: 2203.14923 [hep-ex]. №: FERMILAB-CONF-22-996-PPD-T.
- [80] K. Freese, J. A. Frieman, and A. V. Olinto. ‘Natural inflation with pseudo - Nambu-Goldstone bosons’. In: *Phys. Rev. Lett.* 65 (1990), pp. 3233–3236. DOI: 10.1103/PhysRevLett.65.3233. №: FERMILAB-PUB-90-177-A.
- [81] K. V. Berghaus, P. W. Graham, and D. E. Kaplan. ‘Minimal Warm Inflation’. In: *JCAP* 03 (2020). [Erratum: *JCAP* 10, E02 (2023)], p. 034. DOI: 10.1088/1475-7516/2020/03/034. arXiv: 1910.07525 [hep-ph].
- [82] M. Laine and S. Procacci. ‘Minimal warm inflation with complete medium response’. In: *JCAP* 06 (2021), p. 031. DOI: 10.1088/1475-7516/2021/06/031. arXiv: 2102.09913 [hep-ph].
- [83] P. W. Graham, I. G. Irastorza, S. K. Lamoreaux, A. Lindner, and K. A. van Bibber. ‘Experimental Searches for the Axion and Axion-Like Particles’. In: *Ann. Rev. Nucl. Part. Sci.* 65 (2015), pp. 485–514. DOI: 10.1146/annurev-nucl-102014-022120. arXiv: 1602.00039 [hep-ex].

- [84] P. Sikivie. ‘Invisible Axion Search Methods’. In: *Rev. Mod. Phys.* 93.1 (2021), p. 015004. DOI: 10.1103/RevModPhys.93.015004. arXiv: 2003.02206 [hep-ph].
- [85] A. Blondel et al. ‘Searches for long-lived particles at the future FCC-ee’. In: *Front. in Phys.* 10 (2022), p. 967881. DOI: 10.3389/fphy.2022.967881. arXiv: 2203.05502 [hep-ex].
- [86] C. Antel et al. ‘Feebly Interacting Particles: FIPs 2022 workshop report’. *Workshop on Feebly-Interacting Particles*. May 2023. arXiv: 2305.01715 [hep-ph]. №: CERN-TH-2023-061, DESY-23-050, FERMILAB-PUB-23-149-PPD, INFN-23-14-LNF, JLAB-PHY-23-3789, LA-UR-23-21432, and MITP-23-015.
- [87] G. G. Raffelt. ‘Astrophysical axion bounds’. In: *Lect. Notes Phys.* 741 (2008). Ed. by M. Kuster, G. Raffelt, and B. Beltran, pp. 51–71. DOI: 10.1007/978-3-540-73518-2_3. arXiv: hep-ph/0611350. №: MPP-2006-172.
- [88] A. Arvanitaki and A. A. Geraci. ‘Detecting high-frequency gravitational waves with optically-levitated sensors’. In: *Phys. Rev. Lett.* 110.7 (2013), p. 071105. DOI: 10.1103/PhysRevLett.110.071105. arXiv: 1207.5320 [gr-qc].
- [89] M. Goryachev and M. E. Tobar. ‘Gravitational Wave Detection with High Frequency Phonon Trapping Acoustic Cavities’. In: *Phys. Rev. D* 90.10 (2014). [Erratum: *Phys.Rev.D* 108, 129901 (2023)], p. 102005. DOI: 10.1103/PhysRevD.90.102005. arXiv: 1410.2334 [gr-qc].
- [90] V. Domcke and C. Garcia-Cely. ‘Potential of radio telescopes as high-frequency gravitational wave detectors’. In: *Phys. Rev. Lett.* 126.2 (2021), p. 021104. DOI: 10.1103/PhysRevLett.126.021104. arXiv: 2006.01161 [astro-ph.CO]. №: DESY-20-097 and CERN-TH-2020-082.
- [91] N. Aggarwal, G. P. Winstone, M. Teo, M. Baryakhtar, S. L. Larson, V. Kalogera, and A. A. Geraci. ‘Searching for New Physics with a Levitated-Sensor-Based Gravitational-Wave Detector’. In: *Phys. Rev. Lett.* 128.11 (2022), p. 111101. DOI: 10.1103/PhysRevLett.128.111101. arXiv: 2010.13157 [gr-qc].
- [92] A. Berlin, D. Blas, R. Tito D’Agnolo, S. A. R. Ellis, R. Harnik, Y. Kahn, and J. Schütte-Engel. ‘Detecting high-frequency gravitational waves with microwave cavities’. In: *Phys. Rev. D* 105.11 (2022), p. 116011. DOI: 10.1103/PhysRevD.105.116011. arXiv: 2112.11465 [hep-ph]. №: FERMILAB-PUB-21-724-SQMS-T.
- [93] V. Domcke, C. Garcia-Cely, and N. L. Rodd. ‘Novel Search for High-Frequency Gravitational Waves with Low-Mass Axion Haloscopes’. In: *Phys. Rev. Lett.* 129.4 (2022), p. 041101. DOI: 10.1103/PhysRevLett.129.041101. arXiv: 2202.00695 [hep-ph]. №: DESY-22-017 and CERN-TH-2022-010.
- [94] A. Berlin et al. ‘Electromagnetic cavities as mechanical bars for gravitational waves’. In: *Phys. Rev. D* 108.8 (2023), p. 084058. DOI: 10.1103/PhysRevD.108.084058. arXiv: 2303.01518 [hep-ph]. №: FERMILAB-PUB-22-892-SQMS-T.
- [95] G. Ballesteros, J. Redondo, A. Ringwald, and C. Tamarit. ‘Standard Model—axion—seesaw—Higgs portal inflation. Five problems of particle physics and cosmology solved in one stroke’. In: *JCAP* 08 (2017), p. 001. DOI: 10.1088/1475-7516/2017/08/001. arXiv: 1610.01639 [hep-ph]. №: DESY-16-184, IPPP-16-79, and CERN-TH-2016-055.

- [96] M. Laine, L. Niemi, S. Procacci, and K. Rummukainen. ‘Shape of the hot topological charge density spectral function’. In: *JHEP* 11 (2022), p. 126. DOI: 10.1007/JHEP11(2022)126. arXiv: 2209.13804 [hep-ph].
- [97] M. Drewes. ‘The Phenomenology of Right Handed Neutrinos’. In: *Int. J. Mod. Phys. E* 22 (2013), p. 1330019. DOI: 10.1142/S0218301313300191. arXiv: 1303.6912 [hep-ph]. №: TUM-HEP-881-13.
- [98] A. M. Abdullahi et al. ‘The present and future status of heavy neutral leptons’. In: *J. Phys. G* 50.2 (2023), p. 020501. DOI: 10.1088/1361-6471/ac98f9. arXiv: 2203.08039 [hep-ph]. №: FERMILAB-CONF-22-184-T-V.
- [99] L. Canetti, M. Drewes, and M. Shaposhnikov. ‘Matter and Antimatter in the Universe’. In: *New J. Phys.* 14 (2012), p. 095012. DOI: 10.1088/1367-2630/14/9/095012. arXiv: 1204.4186 [hep-ph]. №: TTK-12-04.
- [100] M. Fukugita and T. Yanagida. ‘Baryogenesis Without Grand Unification’. In: *Phys. Lett. B* 174 (1986), pp. 45–47. DOI: 10.1016/0370-2693(86)91126-3. №: RIFP-641.
- [101] E. K. Akhmedov, V. A. Rubakov, and A. Y. Smirnov. ‘Baryogenesis via neutrino oscillations’. In: *Phys. Rev. Lett.* 81 (1998), pp. 1359–1362. DOI: 10.1103/PhysRevLett.81.1359. arXiv: hep-ph/9803255. №: IC-98-22 and INR-98-14-T.
- [102] T. Asaka and M. Shaposhnikov. ‘The ν MSM, dark matter and baryon asymmetry of the universe’. In: *Phys. Lett. B* 620 (2005), pp. 17–26. DOI: 10.1016/j.physletb.2005.06.020. arXiv: hep-ph/0505013.
- [103] S. Dodelson and L. M. Widrow. ‘Sterile-neutrinos as dark matter’. In: *Phys. Rev. Lett.* 72 (1994), pp. 17–20. DOI: 10.1103/PhysRevLett.72.17. arXiv: hep-ph/9303287. №: FERMILAB-PUB-93-057-A.
- [104] X.-D. Shi and G. M. Fuller. ‘A New dark matter candidate: Nonthermal sterile neutrinos’. In: *Phys. Rev. Lett.* 82 (1999), pp. 2832–2835. DOI: 10.1103/PhysRevLett.82.2832. arXiv: astro-ph/9810076.
- [105] B. Garbrecht. ‘Why is there more matter than antimatter? Computational methods for leptogenesis and electroweak baryogenesis’. In: *Prog. Part. Nucl. Phys.* 110 (2020), p. 103727. DOI: 10.1016/j.pnpnp.2019.103727. arXiv: 1812.02651 [hep-ph]. №: TUM-HEP-1177-18.
- [106] J. Klarić, M. Shaposhnikov, and I. Timiryasov. ‘Reconciling resonant leptogenesis and baryogenesis via neutrino oscillations’. In: *Phys. Rev. D* 104.5 (2021), p. 055010. DOI: 10.1103/PhysRevD.104.055010. arXiv: 2103.16545 [hep-ph].
- [107] M. Drewes et al. ‘A White Paper on keV Sterile Neutrino Dark Matter’. In: *JCAP* 01 (2017), p. 025. DOI: 10.1088/1475-7516/2017/01/025. arXiv: 1602.04816 [hep-ph]. №: FERMILAB-PUB-16-068-T.
- [108] A. Boyarsky, M. Drewes, T. Lasserre, S. Mertens, and O. Ruchayskiy. ‘Sterile neutrino Dark Matter’. In: *Prog. Part. Nucl. Phys.* 104 (2019), pp. 1–45. DOI: 10.1016/j.pnpnp.2018.07.004. arXiv: 1807.07938 [hep-ph].

- [109] S. Biondini et al. ‘Status of rates and rate equations for thermal leptogenesis’. In: *Int. J. Mod. Phys. A* 33.05n06 (2018), p. 1842004. DOI: 10.1142/S0217751X18420046. arXiv: 1711.02864 [hep-ph].
- [110] B. Garbrecht, P. Klose, and C. Tamarit. ‘Relativistic and spectator effects in leptogenesis with heavy sterile neutrinos’. In: *JHEP* 02 (2020), p. 117. DOI: 10.1007/JHEP02(2020)117. arXiv: 1904.09956 [hep-ph]. №: TUM-HEP-1198-19 and CP3-19-18.
- [111] G. F. Giudice, M. Peloso, A. Riotto, and I. Tkachev. ‘Production of massive fermions at preheating and leptogenesis’. In: *JHEP* 08 (1999), p. 014. DOI: 10.1088/1126-6708/1999/08/014. arXiv: hep-ph/9905242. №: CERN-TH-99-117.
- [112] M. Shaposhnikov and I. Tkachev. ‘The nuMSM, inflation, and dark matter’. In: *Phys. Lett. B* 639 (2006), pp. 414–417. DOI: 10.1016/j.physletb.2006.06.063. arXiv: hep-ph/0604236. №: CERN-PH-TH-2006-069.
- [113] V. Domcke. ‘Electromagnetic high-frequency gravitational wave detection’. *57th Rencontres de Moriond on Electroweak Interactions and Unified Theories*. June 2023. arXiv: 2306.04496 [gr-qc]. №: CERN-TH-2023-099.
- [114] M. Giovannini. ‘The maximal frequency of cosmic gravitons’ (Nov. 2023). arXiv: 2311.17725 [gr-qc].
- [115] M. Giovannini. ‘Relic gravitons and high-frequency detectors’. In: *JCAP* 05 (2023), p. 056. DOI: 10.1088/1475-7516/2023/05/056. arXiv: 2303.11928 [gr-qc].
- [116] N. Herman, L. Lehoucq, and A. Füzfa. ‘Electromagnetic Antennas for the Resonant Detection of the Stochastic Gravitational Wave Background’ (Mar. 2022). arXiv: 2203.15668 [gr-qc].
- [117] P. Navarro, B. Gimeno, J. Monzón-Cabrera, A. Díaz-Morcillo, and D. Blas. ‘Study of a cubic cavity resonator for gravitational waves detection in the microwave frequency range’ (Dec. 2023). arXiv: 2312.02270 [hep-ph].
- [118] S. F. King, S. Pascoli, J. Turner, and Y.-L. Zhou. ‘Confronting $SO(10)$ GUTs with proton decay and gravitational waves’. In: *JHEP* 10 (2021), p. 225. DOI: 10.1007/JHEP10(2021)225. arXiv: 2106.15634 [hep-ph]. №: IPPP/20/120.
- [119] B. Fu, S. F. King, L. Marsili, S. Pascoli, J. Turner, and Y.-L. Zhou. ‘Testing Realistic $SO(10)$ SUSY GUTs with Proton Decay and Gravitational Waves’ (Aug. 2023). arXiv: 2308.05799 [hep-ph]. №: IPPP/23/41.
- [120] A. Anisimov, D. Besak, and D. Bodeker. ‘Thermal production of relativistic Majorana neutrinos: Strong enhancement by multiple soft scattering’. In: *JCAP* 03 (2011), p. 042. DOI: 10.1088/1475-7516/2011/03/042. arXiv: 1012.3784 [hep-ph]. №: BI-TP-2010-48.
- [121] L. J. Hall, K. Jedamzik, J. March-Russell, and S. M. West. ‘Freeze-In Production of FIMP Dark Matter’. In: *JHEP* 03 (2010), p. 080. DOI: 10.1007/JHEP03(2010)080. arXiv: 0911.1120 [hep-ph]. №: OUTP-09-18-P and UCB-PTH-09-32.
- [122] A. Tokareva. ‘Gravitational Waves from Inflaton Decay and Bremsstrahlung’ (Dec. 2023). arXiv: 2312.16691 [hep-ph].

- [123] A. Tokareva. ‘Ultra-high frequency gravitational waves from inflaton decay. Ultra-high frequency gravitational waves: where to next ?’ (2023). URL: cds.cern.ch/record/2883492.
- [124] J. M. Cornwall, R. Jackiw, and E. Tomboulis. ‘Effective Action for Composite Operators’. In: *Phys. Rev. D* 10 (1974), pp. 2428–2445. DOI: [10.1103/PhysRevD.10.2428](https://doi.org/10.1103/PhysRevD.10.2428). №: MIT-CTP-419.
- [125] T. Prokopec, M. G. Schmidt, and S. Weinstock. ‘Transport equations for chiral fermions to order \hbar and electroweak baryogenesis. Part 1’. In: *Annals Phys.* 314 (2004), pp. 208–265. DOI: [10.1016/j.aop.2004.06.002](https://doi.org/10.1016/j.aop.2004.06.002). arXiv: [hep-ph/0312110](https://arxiv.org/abs/hep-ph/0312110). №: BNL-72343-2004-JA and HD-THEP-03-62.
- [126] J. Berges. ‘Nonequilibrium Quantum Fields: From Cold Atoms to Cosmology’ (Mar. 2015). arXiv: [1503.02907](https://arxiv.org/abs/1503.02907) [hep-ph].
- [127] B. Garbrecht and M. Garny. ‘Finite Width in out-of-Equilibrium Propagators and Kinetic Theory’. In: *Annals Phys.* 327 (2012), pp. 914–934. DOI: [10.1016/j.aop.2011.10.005](https://doi.org/10.1016/j.aop.2011.10.005). arXiv: [1108.3688](https://arxiv.org/abs/1108.3688) [hep-ph]. №: TTK-11-37 and TUM-HEP-816-11.
- [128] M. Drewes, S. Mendizabal, and C. Weniger. ‘The Boltzmann Equation from Quantum Field Theory’. In: *Phys. Lett. B* 718 (2013), pp. 1119–1124. DOI: [10.1016/j.physletb.2012.11.046](https://doi.org/10.1016/j.physletb.2012.11.046). arXiv: [1202.1301](https://arxiv.org/abs/1202.1301) [hep-ph]. №: MPP-2012-3, TTK-12-03, and TUM-HEP-857-12.
- [129] Y.-K. E. Cheung, M. Drewes, J. U. Kang, and J. C. Kim. ‘Effective Action for Cosmological Scalar Fields at Finite Temperature’. In: *JHEP* 08 (2015), p. 059. DOI: [10.1007/JHEP08\(2015\)059](https://doi.org/10.1007/JHEP08(2015)059). arXiv: [1504.04444](https://arxiv.org/abs/1504.04444) [hep-ph].
- [130] G. Buldgen, M. Drewes, J. U. Kang, and U. R. Mun. ‘General Markovian equation for scalar fields in a slowly evolving background’. In: *JCAP* 05.05 (2022), p. 039. DOI: [10.1088/1475-7516/2022/05/039](https://doi.org/10.1088/1475-7516/2022/05/039). arXiv: [1912.02772](https://arxiv.org/abs/1912.02772) [hep-ph]. №: CP3-19-54.
- [131] V. V. Klimov. ‘Collective Excitations in a Hot Quark Gluon Plasma’. In: *Sov. Phys. JETP* 55 (1982), pp. 199–204.
- [132] H. A. Weldon. ‘Effective Fermion Masses of Order gT in High Temperature Gauge Theories with Exact Chiral Invariance’. In: *Phys. Rev. D* 26 (1982), p. 2789. DOI: [10.1103/PhysRevD.26.2789](https://doi.org/10.1103/PhysRevD.26.2789). №: PRINT-82-0423 (PENN).